



Enhancement of R123 Pool Boiling by the Addition of Hydrocarbons

Mark A. Kedzierski

U.S. DEPARTMENT OF COMMERCE
Technology Administration
National Institute of Standards
and Technology
Building and Fire Research Laboratory
Gaithersburg, MD 20899

QC
100
.U56
NO.6244
1998



Enhancement of R123 Pool Boiling by the Addition of Hydrocarbons

Mark A. Kedzierski

U.S. DEPARTMENT OF COMMERCE
Technology Administration
National Institute of Standards
and Technology
Building and Fire Research Laboratory
Gaithersburg, MD 20899

October 1998



U.S. DEPARTMENT OF COMMERCE
William M. Daley, Secretary

TECHNOLOGY ADMINISTRATION
Gary R. Bachula, Acting Under Secretary
for Technology

NATIONAL INSTITUTE OF STANDARDS
AND TECHNOLOGY
Raymond G. Kammer, Director

U.S. DEPARTMENT OF ENERGY
Washington, D.C. 20858

ABSTRACT

This paper presents pool boiling heat transfer data for ten different R123/hydrocarbon mixtures. The data consisted of pool boiling performance of a GEWA-T™ surface for pure R123 and for ten dilute solutions of five different hydrocarbons: (1) pentane, (2) isopentane, (3) hexane, (4) cyclohexane, and (5) heptane with R123. The heat flux and the wall superheat were measured for each fluid at 277.6 K. A maximum (19 ± 3.5)% increase over the pure R123 heat flux was achieved with the addition of 0.5% mass isopentane to R123. Other mixtures of isopentane, pentane, hexane, and cyclohexane with R123 exhibited smaller maximums than that of the R123/isopentane (99.5/0.5) mixture. Presumably, a layer enriched in hydrocarbon at the heat transfer surface caused the heat transfer enhancement. Conversely, an R123/heptane (99.5/0.5) mixture and an R123/cyclohexane (99.5/0.5) mixture exhibited only degradations with respect to the pure component performance for all test conditions. Several characteristics of the hydrocarbons were examined to determine their influence on the boiling heat transfer performance: molecular weight, molecular structure, composition, surface tension, and vapor pressure.

Keywords: Additive, binary mixtures, enhanced heat transfer, fluid heating, GEWA-T™, hydrocarbons, pool boiling, R123, refrigerants, surfactant

INTRODUCTION

Typically, binary mixtures exhibit a boiling performance degradation compared to their pure components (Shock, 1982 and Thome, 1990). Yet, some special liquids, when added in small quantities, enhance the boiling performance of pure fluids. For the refrigeration and air-conditioning industry, a liquid additive would be an economical means of reducing manufacturing and/or operating costs. For example, a liquid additive for 1,1-dichloro-2,2,2-trifluoroethane (R123) would enable existing water chillers to operate more efficiently or enable new water chillers to meet the same duty with fewer tubes. Unfortunately, liquid additives that significantly enhance refrigerant boiling performance are rare.

Most of the work on liquid additives has been in surfactants for aqueous solutions (Jontz and Myers (1960), Shah and Darby (1973) and Wu et al. (1995)). Carey (1992) and Rosen (1978) describe how surfactants reduce the surface tension of water. Basically, the surfactant molecule must have polar and nonpolar ends, i.e., an amphipathic structure. The nonpolar end of the surfactant distorts the interior structure of the solution. The structural distortion allows a surfactant molecule to travel to the liquid-vapor interface with less work than is required to bring a water molecule to the surface. By definition, the surface tension of the liquid-vapor interface is lowered when less work is required to bring a molecule to the surface.

Not much research has been done on surfactants for refrigerants. Kedzierski (1999) measured a significant enhancement of R123 pool boiling with the addition of 1% and 2% hexane by mass to R123. He used the Gibbs adsorption equation and the Young and Dupre equation to speculate that the boiling heat transfer enhancement of R123 by the addition of hexane was caused by an accumulation of hydrocarbon at the boiling surface. In essence, the greater concentration of hydrocarbon or “excess layer” at the heat transfer surface caused a reduction of the surface energy between the solid surface and the liquid. The existence of an excess layer at the liquid-solid interface is analogous to the existence of a surfactant induced excess layer at a liquid-vapor interface. Consequently, the hydrocarbon is not a typical surfactant because it accumulates at the solid-liquid interface rather than the liquid-vapor interface. However, the reduction in the liquid-solid surface energy results in a similar reduction in bubble departure diameter that occurs with a conventional surfactant. As a consequence of the bubble size reduction, the active site density increases. A heat transfer enhancement existed when a favorable balance between an increase in site density and a reduction in bubble size occurs.

In the present study, five different hydrocarbons were tested as additives in various concentrations with R123 in an effort to investigate the enhancement mechanism of the excess layer. The various hydrocarbons were chosen for their wide range of properties: namely, normal boiling point, interfacial surface tension, molecular weight, and molecular structure. It was hypothesized that certain thermophysical and chemical properties of the hydrocarbon were favorable for the creation of an excess layer. For example, an R123/hydrocarbon mixture that behaved as an azeotrope in the bulk mixture would be more likely to exhibit a heat transfer enhancement with respect to pure R123. For an azeotropic mixture, the excess layer is formed due to the strong affinity of the hydrocarbon for the solid surface. Dilute solution of hydrocarbons with R123 and mixture of components with similar boiling points were unlikely to exhibit heat transfer degradations that can be associated with concentration gradients. It was also

believed that a large difference between the surface tension of the additive and the refrigerant would create a large potential to reduce the surface energy of the liquid-solid interface via the excess layer. The stability of the excess layer may rely on the molecular structure of the hydrocarbon. For example, a particular molecular structure of a hydrocarbon may be more conducive to the formation of an excess layer due to its degree of repulsion of the polar R123 molecules that are at the interface of the excess layer and the bulk liquid.

APPARATUS

Figure 1 shows a schematic of the apparatus that was used to measure the pool boiling data of this study. More specifically, the apparatus was used to measure the liquid saturation temperature (T_s), the average pool-boiling heat flux (q''), and the wall temperature (T_w) of the test surface at the root of the fin. The three principal components of the apparatus were test chamber, condenser, and purger. The internal dimensions of the test chamber were 25.4 mm \times 257 mm \times 1.54 m. The test chamber was charged with approximately 7 kg of R123 from the purger, giving a liquid height of approximately 80mm above the test surface. As shown in Fig. 1, the test section was visible through two opposing, flat 150 mm \times 200 mm quartz windows. The bottom of the test surface was heated with high velocity (2.5 m/s) water flow. The vapor produced by liquid boiling on the test surface was condensed by the brine-cooled, shell-and-tube condenser and returned as liquid to the pool by gravity.

To reduce the errors associated with the liquid saturation temperature measurement, the saturation temperature of the liquid was measured with two 450 mm long 1.6 mm diameter stainless steel sheathed thermocouples. The small diameter provided for a relatively rapid response time. Nearly the entire length of the thermocouple was in contact with either the test refrigerant vapor or liquid to minimize conduction errors. The tip of the two thermocouples were placed approximately 2 mm above and 150 mm (and 300 mm) to one side of the top of the test surface. This placement ensured that approximately 80 mm of the probe length was in relatively well-mixed liquid near the two-phase fluid above the test surface. To provide for a saturated liquid pool state, the mass of liquid in the pool was large compared to mass of liquid condensed. At the highest heat flux, it would require nearly one hour to evaporate and condense the entire test chamber charge. The lack of a temperature difference between the probe and the well-insulated, low emissivity, 38 mm aluminum test chamber walls essentially eliminated temperature errors due to radiation to the probe.

TEST SURFACE

Figure 2 shows the oxygen-free high-conductivity (OFHC) copper GEWA-TTM test plate used in this study. Commercially, flattening the tips of the GEWA-KTM surface forms the GEWA-TTM or "T-fin" surface. The GEWA-TTM surface in this study was machined directly onto the top of the test plate by electric discharge machining (EDM). Figure 3 shows a photograph of the fin surface. The gap between the fin-tips was 0.348 mm. The surface had approximately 667 fins per meter oriented along the short axis of the plate. The ratio of the surface area to the projected area of the surface was 2.47. The fin-tip width and the fin-height were 1.05 mm and 1.038 mm, respectively.

MEASUREMENTS AND UNCERTAINTIES

The standard uncertainty (u_i) is the positive square root of the estimated variance u_i^2 . The individual standard uncertainties are combined to obtain the expanded uncertainty (U). The expanded uncertainty is commonly referred to as the law of propagation of uncertainty with a coverage factor. All measurement uncertainties are reported for a 95% confidence interval.

The copper-constantan thermocouples and the data acquisition system were calibrated against a glass-rod standard platinum resistance thermometer (SPRT) and a reference voltage to a residual standard deviation of 0.005 K. The NIST Thermometry Group calibrated the fixed SPRT to two fixed points having expanded uncertainties of 0.06 mK and 0.38 mK. A quartz thermometer, which was calibrated with a distilled ice bath, agreed with the SPRT temperature to within approximately 0.003 K. Both the measured thermocouple electromotive force (EMF) and the measured 1 mV reference were regressed to the SPRT temperature. During a pool-boiling test, the 1 mV reference was measured prior to measuring each thermocouple EMF. The reference voltage was used to account for the drift in the acquisition measurement capabilities over time. Before each test run, the measurements of a thermocouple in the bath with the SPRT were compared. The mean absolute difference between the thermocouple and the SPRT was 0.06 K over one year. Considering the fluctuations in the saturation temperature during the test and the standard uncertainties in the calibration, the expanded uncertainty of the average saturation temperature was no greater than 0.04 K. Consequently, it is believed that the expanded uncertainty of the temperature measurements was less than 0.1 K. The saturation temperature was also obtained from a pressure transducer measurement with an uncertainty of less than 0.03 kPa. The uncertainty of the saturation temperature from a regression (with a residual standard deviation of 0.6 mK) of equilibrium data (Morrison and Ward, 1991) for R123 was 0.17 K. The saturation temperature obtained from the thermocouple and the pressure measurement nearly always agreed within ± 0.17 K for the pure R123 data.

Figure 2 shows the coordinate system for the 20 wells where individual thermocouples were force fitted into the side of the test plate. The wells were 16 mm deep to reduce conduction errors. Using a method given by Eckert and Goldstein (1976), errors due to heat conduction along the thermocouple leads were estimated to be well below 0.01 mK. The origin of the coordinate system was centered on the surface with respect to the y-direction at the root of the fin. Centering the origin in the y-direction improved the accuracy of the wall heat flux and temperature calculations by reducing the number of fitted constants involved in these calculations. The x-coordinate measures the distance normal to the heat transfer surface. The y-coordinate measures the distance perpendicular to the x-coordinate. The thermocouples were arranged in four sets of five aligned in the x-direction. Following a procedure given by Kedzierski and Worthington (1993), the size and arrangement of the thermocouple wells were designed to minimize the errors in the wall temperature and temperature gradient measurement.

The heat flux and the wall temperature were obtained by regressing the measured temperature distribution of the block to the governing two-dimensional conduction equation (Laplace equation). In other words, rather than using the boundary conditions to solve for the interior temperatures, the interior temperatures were used to solve for the boundary conditions following a backward stepwise procedure given in Kedzierski (1995).

A backward stepwise regression was used to determine the best model or the significant terms of the solution to the Laplace equation in rectangular coordinates for each data point. Most infinite series solutions should converge within nine terms. The backward stepwise method began by regressing the first nine terms of the Laplace infinite series solution to the twenty measured plate temperatures:

$$T = A_0 + A_1x + B_1y + A_2(x^2 - y^2) + 2B_2xy + A_3x(x^2 - 3y^2) + B_3y(3x^2 - y^2) + A_4(x^4 - 6x^2y^2 + y^4) + 4B_4(x^3y - xy^3) \quad 1$$

The above "full" model was reduced to its significant terms by removing terms with t-values less than two while maintaining the original residual standard deviation of the full model. Terms were removed one at a time. Regression of the 20 temperatures was done after each term with the smallest t-values was removed. Table 1 provides an overview of the various two-dimensional conduction models that were used to reduce the measured temperatures to heat fluxes and wall temperatures.

Fourier's law and the fitted constants (A_0, A_1, \dots, A_n) were used to calculate the average heat flux (q'') normal to and evaluated at the heat transfer surface as:

$$q'' = \left(\frac{1}{L_y} \int_{-\frac{L_y}{2}}^{\frac{L_y}{2}} k \frac{\partial T}{\partial x} dy \right)_{x=0} = \bar{k} A_1 \quad 2$$

where \bar{k} is the average thermal conductivity along the surface of the plate, and L_y is the length of the heat transfer surface as shown in Fig. 2.

The average wall temperature (T_w) was calculated by integrating the local wall temperature:

$$T_w = \left(\frac{1}{L_y} \int_{-\frac{L_y}{2}}^{\frac{L_y}{2}} T dy \right)_{x=0} = A_0 \quad 3$$

Siu et al. (1976) estimated the uncertainty in the thermal conductivity of OFHC copper to be about 2% to 3% by comparing round-robin experiments. Considering this, the relative expanded uncertainty in q'' was greatest at the lowest heat fluxes, approaching 10% of the measurement at 10 kw/m². In general, the $E_{q''}$ appears to be relatively constant between 6% and 3% for heat fluxes above 30,000 W/m². The average random error in the wall superheat -- ($\Delta T_s = \overline{T_w} - T_s$)-- was within 0.1 K. A more detailed discussion of the uncertainty analysis can be found in Kedzierski (1996). After the data was reduced, it was realized that only one of the two thermocouples used to measure the liquid saturation temperature was used to calculate the wall superheat. This oversight may have added approximately 0.05 K to the systematic error. Considering that the boiling curve may drift more than 0.05 K in a month due to surface aging,

the shift in superheat was considered to be inconsequential due to the comparative purpose of the study.

EXPERIMENTAL RESULTS

The heat flux was varied from 80 kW/m^2 to 10 kW/m^2 to simulate typical operating conditions of R123 chillers equipped with enhanced tubes. All pool boiling tests were taken at 277.6 K saturated conditions. The data were recorded consecutively starting at approximately 80 kW/m^2 and then descending to 10 kW/m^2 in intervals of approximately 4 kW/m^2 . The descending heat flux procedure minimized the possibility of any hysteresis effects on the data, which would have made the data sensitive to the initial operating conditions. Table 2 presents the measured heat flux and wall superheat for all of the data of this study. Table 3 gives the number of test days and data points for each fluid.

The mixtures were prepared by first charging approximately 90% of the R123 into the test chamber to a known mass. Next, measured weights of the particular spectrophotometric grade hydrocarbon were injected through a valve in the side of the test chamber (see Fig. 1). The liquid hydrocarbon was injected with a syringe through the valve, followed by flushing with the remaining R123 charge. The flushing of R123 through the valve and connecting tubes also assisted in mixing the charge. All compositions are determined from the masses of the charged components and are given on a mass percent basis. The maximum uncertainty of the composition measurement is approximately 0.02%, e.g. the range of a 0.5% composition is between 0.48% and 0.52%.

The pool boiling performance of dilute mixtures of R123 and the following hydrocarbons were measured at 0.5% and 1.0% by mass hydrocarbon: isopentane, pentane, hexane, and cyclohexane. An R123/isopentane (99.5/0.5) by mass mixture was also tested along with an R123/heptane (99.9/0.1) by mass mixture. Pure R123 pool boiling data was taken to provide a baseline for comparison to the mixtures.

Figures 4 through 14 are plots of the measured heat flux (q'') versus the measured wall superheat ($T_w - T_s$) for all of the fluids. On average, each fluid was tested over six days. For the most part, one day's test covered heat fluxes from 80 kW/m^2 to 10 kW/m^2 . The solid line is a cubic best-fit regression or estimated mean of the data. Two cubic fits were required to cover the low and the high heat flux data. Table 4 gives the constants for the cubic regression of the superheat versus the heat flux for each test fluid. The residual standard deviation of the regressions - representing the proximity of the data to the mean - are given in Table 5. On average, the residual standard deviation of the low heat flux and the high heat flux data about the mean is 0.17 K and 0.10 K, respectively. The dashed lines to either side of the mean represent the lower and upper 95% simultaneous (multiple-use) confidence intervals for the mean. The expanded uncertainty of the estimated mean wall superheat in the low heat flux region and the high heat flux region is approximately 0.1 K and 0.07 K, respectively. Table 6 provides the average mean wall uncertainty for low and high heat fluxes.

Figure 4 presents the boiling curve for pure R123 at 277.6 K on the GEWA-TTM surface. The boiling curve exhibits two characteristic regimes: a natural convection/boiling regime and a

vigorous nucleate boiling regime. The regimes are separated by the cessation of vigorous nucleate boiling (CVNB). The CVNB occurs for the pure R123 data at approximately 9.5 K (24 kW/m^2). The nucleate boiling regime exists for superheats that are greater than the CVNB condition. Here, the heat transfer is governed primarily by the formation of isolated bubbles within the fin cavities. The superheats below the CVNB are insufficient to support vigorous bubble generation. Consequently, natural convection becomes a prevalent mode of heat transfer for superheats below CVNB. In this region, limited bubble activity exists.

Figure 4 compares the present R123 GEWA-TTM boiling curve to R123 GEWA-TTM boiling data that was taken approximately five years prior (Kedzierski, 1999) to the present data in the same apparatus and for the same surface. The data differ substantially in the vigorous boiling region, but agree closely in the natural convection/boiling region. Apparently, the surface condition has changed such that many nucleation sites have been eliminated. The surface was stored in a felt-lined wooden box for the years between testing. The surface was cleaned prior to installation in the test apparatus with acetone, TarnexTM, hot tap water, and acetone for both the 1993 and the present tests. Following the cleaning process, the surface was exposed to a heat lamp for several hours. Just prior to the present tests, the surface was used for active pool boiling testing for nearly two years after the storage period. Aging and/or fouling of the surface have produced an offset in the wall superheat of approximately 2 K. It is believed that the superheat offset is not caused by a malfunctioning of the test equipment because no equivalent offset between the measured saturation temperature and the saturation temperature obtained from the measured pressure was observed. Also, the agreement of low heat flux data for the two periods shows that the measurements are consistent. In addition, examination of the surface after the present tests revealed that it was fouled with a somewhat tacky substance. The surface may have been contaminated with decane from previous R123/decane pool boiling tests. The decane could have been adsorbed on the test surface in a manner similar to that, which was observed by Tamura et al. (1983) where surfactants were irreversible adsorbed on metal surfaces.

Figure 4 also compares the NIST 1993 GEWA-TTM boiling curve to GEWA-TXTM boiling curve measured by Webb and Pais (1992) at equal saturation temperatures. The figure summarizes the geometrical differences between the plate tested in this study and the tube that Webb and Pais (1992) tested. The Webb and Pais (1992) GEWA-TXTM data agree with the 1993 data for heat fluxes above 64 kW/m^2 and at 10 kW/m^2 and is greater than the present data for intermediate heat fluxes. The maximum percent difference between the two data sets of 100% occurs at the CVNB.

The greater performance of the Webb and Pais (1992) GEWA-TXTM surface compared to the 1993 NIST data for the intermediate heat flux region was partly due to the greater fins-per-meter (fpm) and the additional notch enhancement of the GEWA-TXTM surface. Also, the gap between the fins (S_f) on the plate was significantly larger than that on the GEWA-TXTM tube. The smaller fin-gap and the notch are effective at enhancing heat transfer at low site densities. A narrower fin-gap encourages bubble coalescence within the cavity. The notch acts to increase the site density. As the site density increases with the heat flux and the surface becomes saturated with bubbles, these geometry effects become less effective at heat transfer enhancement. Also, a flat plate does not experience the convection, as reported by Cornwell and

Einarsson (1989), that is induced by bubbles that slide within the channels of the side of a tube. The sliding bubbles also act to seed upper portions of the tube with vapor. These mechanisms would be less influential at higher heat fluxes where most of the potential sites have become active with vigorous bubble activity. Consequently, the performance difference between the plate and the tube becomes less significant at larger heat fluxes.

Figure 4 also shows the predictions from a free convection correlation for a horizontal plate with the upper surface being heated which was recommended by Incropera and Dewitt (1985). Although the correlation is for a flat plate, it may be possible to account for the enhanced surface with the characteristic length defined as the surface area over the exterior perimeter of the plate. The predictions are substantially lower than the present measurements. This is consistent with the enhancement of the free convection by some nucleate boiling and the upward motion of bubbles.

Figures 5 through 14 show the boiling curve for each of the mixtures in this study. As was done for pure R123, the cubic regressions are shown as solid lines. Dotted lines depict the 95% simultaneous confidence intervals for the cubic fits. A cubic fit for the high and low heat flux regions were required for each mixture. The following discussion examines the relative heat transfer performance of the mixtures and that of pure R123.

Figures 15 through 20 illustrate the effect of the addition of the various hydrocarbons to R123 on heat transfer performance. The figures plot the ratio of the mixture to the pure R123 heat flux (q''_m/q''_p) versus the pure R123 heat flux (q''_p) at the same wall superheat. A heat transfer enhancement exists where the heat flux ratio is greater than one and the 95% simultaneous confidence intervals (depicted by shaded regions) do not include the value one.

Figure 15 shows that the R123/isopentane (99.5/0.5) mixture exhibits an enhancement for heat fluxes greater than approximately 24 kW/m^2 . The CVNB is located near 24 kW/m^2 . Consequently, the addition of isopentane to R123 improves the heat transfer associated with vigorous boiling more so than it does for low-active-site-density boiling region. The maximum heat flux ratio for the 99.5/0.5 mixture was 1.19 at 50 kW/m^2 . The average heat flux ratio for the R123/isopentane (99.5/0.5) mixture over the entire range of test heat fluxes was 1.10. The performance of the R123/isopentane (99/1) mixture is similar to that of the R123/isopentane (99.5/0.5) mixture but it has a higher uncertainty. The R123/isopentane (99.9/0.1) mixture shows a maximum near its CVNB and decreases for heat fluxes above the CVNB. For 99.5% confidence, no difference exists between the boiling performance of the 99.9/0.1 mixture and pure R123 for heat fluxes greater than 37 kW/m^2 .

Figure 16 shows that the R123/pentane (99.5/0.5) and (99/1) mixtures have similar heat flux ratio profiles. For example, both mixtures exhibit an enhancement for heat fluxes less than approximately 24 kW/m^2 and a degradation for heat fluxes greater than approximately 24 kW/m^2 . Consequently, the addition of pentane to R123 enhances the low-active-site-density region rather than the vigorous boiling region. The maximum heat flux ratio for the R123/pentane (99/1) mixture was 1.14 at 12.6 kW/m^2 . The average heat flux ratio for the R123/pentane (99/1) mixture over the entire range of test heat fluxes was 0.98. The

performance of the R123/pentane (99.5/0.5) mixture is similar to that of the R123/pentane (99/1) mixture but slightly less over nearly the entire heat flux range. The R123/pentane (99.5/0.5) mixture had a maximum heat flux ratio of 1.08 and an overall average heat flux ratio of 0.94.

Figure 17 shows the heat flux ratio for the R123/hexane (99.5/0.5) and R123/hexane (99/1) mixtures. The R123/hexane (99/1) mixture exhibits a maximum heat flux ratio of 1.13 in the low-active-site-density region at 24.4 kW/m^2 . Whereas, the R123/hexane (99.5/0.5) mixture exhibits a maximum heat flux ratio of 1.08 in the vigorous nucleate boiling region (41.8 kW/m^2). The average heat flux ratio for the entire test range was 1.04 and 1.01 for the R123/hexane (99.5/0.5) mixture and the R123/hexane (99/1) mixture, respectively. For 99.5% confidence, the R123/hexane (99.5/0.5) mixture boiling performance does not differ from that of pure R123 for heat fluxes greater than approximately 24 kW/m^2 .

Figure 18 shows data for an R123/hexane (99/1) mixture and an R123/hexane (98/2) mixture that were taken in 1993 (Kedzierski, 1999) on the same surface and the same apparatus that was used in the present study. The R123/hexane (99/1) mixtures for the present study and the 1993 study exhibit a maxima at the same heat flux. However, the magnitude of the heat flux ratio for the 1993 study is much greater than that of the present study. Recall that Fig. 4 showed that the pure R123 boiling curve of the 1993 study significantly differed in the high heat flux region from the previous study. Obviously, the surface characteristics of the GEWA-T™ test plate were altered in the five years between the 1993 study and the present study. Presumably, the surface characteristics play a role in determining the effectiveness of the hydrocarbon in enhancing the active site density for nucleate boiling. From this, it is suspected that the heat flux ratios presented in this study would not be universally applicable to other enhancement geometries.

Figure 19 shows that the addition of heptane by 5% mass to R123 causes a heat transfer degradation for heat fluxes from 15 kW/m^2 to 70 kW/m^2 . The maximum heat flux ratio for the R123/heptane (99.5/0.5) mixture is 0.94 and occurs at 17 kW/m^2 . The heat flux ratio steadily decreases with increasing heat flux to approximately 0.51 at 70 kW/m^2 .

Figure 20 shows the heat flux ratio for two mixtures of R123 and cyclohexane. The R123/cyclohexane (99.5/0.5) mixture exhibits a heat transfer degradation as compared to pure R123 for the entire heat flux range of the tests. The R123/cyclohexane (99/1) has nearly the same performance of the (99.5/0.5) mixture with the exception of a small enhancement ($q''_m/q''_p = 1.04$) at $q''_p = 21.7 \text{ kW/m}^2$.

ENHANCEMENT TRENDS

The following five parameters were investigated for their influence on the boiling heat transfer performance of the hydrocarbon/R123 mixture: (1) the molecular weight of the hydrocarbon; (2) the difference in the boiling points of pure components at 39.8 kPa ($T_h - T_p$); (3) the difference in surface tension between the hydrocarbon and R123 at 277.6 K ($\sigma_h - \sigma_p$); (4) the mixture composition; and (5) the molecular structure of the hydrocarbon. Presumably, these parameters govern the dynamics of the formation of the excess layer for the R123/hydrocarbon mixtures. The mixtures should behave azeotropically in the bulk mixture. For very dilute solutions, mixtures may have large difference in normal boiling points while still maintaining azeotropic

behavior (Lunger and Shealy, 1994). However, due to its affinity for the solid, the hydrocarbon comes out of solution to form a confined region of higher hydrocarbon concentration at the wall. The initial formation of the excess layer due to the affinity of the hydrocarbon for the solid surface causes a composition shift past the azeotropic composition that may further increase the excess concentration through preferential boiling of the refrigerant. In addition, the excess layer cannot form on the wall unless the surface tension of the hydrocarbon is greater than that of R123. Otherwise, the hydrocarbon will act as a surfactant by accumulating at the liquid-vapor interface.

In figures 21 through 26, a linear model was used to provide only an approximate description of the trends in the data. Consequently, nearly each plot contains one or two influential points (Belsley et al., 1980) that may be considered outliers for the linear model. Future research might focus on gathering more data to better describe these trends and to identify the cause of outliers from the apparent linear trends.

Figure 21 shows the heat flux ratio as a function of the molecular weight of the hydrocarbon in the R123/hydrocarbon mixture. In general, larger heat flux ratios are obtained for R123/hydrocarbon mixtures that have hydrocarbons with smaller molecular weights. Hydrocarbons with large molecular weights tend to “be sticky” or have a strong affinity for the solid surface. For this case, the thickness of the excess layer may act as fouling rather than a surfactant for the surface.

Also, Hydrocarbons with large molecular weights tend to have larger vapor pressures relative to R123. Figure 22 illustrates the same point with the difference in boiling points (at 277.6 K) rather than the molecular weight. An R123/hydrocarbon mixture with a large vapor pressure difference or difference in boiling points will more likely exhibit azeotropic behavior, which can lead to a degradation in the heat transfer (Kedzierski et al., 1992). For example, it is likely that the performance of the R123/heptane (99.5/0.5) mixture suffers due to concentration gradients in the liquid.

Figure 23 provides the heat flux ratio as a function of the difference between the surface tension of the pure hydrocarbon (σ_h) and that of the pure R123 (σ_p) at 277.6 K. The figure shows that larger heat flux ratios are associated with smaller differences in surface tension between the hydrocarbon and R123. For a binary mixture, an excess layer is a consequence of differences in surface tension between the component liquids. An additive becomes a liquid-vapor surfactant if its surface tension is less than that of the solute. For this case, the additive accumulates (forms an excess layer) at the liquid-vapor interface and lowers its surface tension. Conversely, if the surface tension of the additive is greater than that of the solute, the additive forms an excess layer at the solid-liquid interface. Here, the surface energy between the liquid and solid is reduced by the presence of the excess layer on the liquid-solid interface. Closer examination of Fig. 22 shows that isopentane may lower the surface tension of the liquid-vapor interface, while the other hydrocarbons may lower the surface tension of the liquid-solid interface. An excess layer at the liquid-vapor interface or one at the liquid-solid interface would produce the same result by different means. That is, a reduction in the surface-tension of either the liquid-vapor or the liquid-solid interface causes a reduction in the bubble contact angle which, in turn, can cause an

enhancement of the heat transfer (Kedzierski, 1999). Nevertheless, the difference between the surface tension of isopentane and R123 may be within the uncertainty of its prediction. Consequently, it is possible that all of the hydrocarbons act on the liquid-solid interface.

Figure 24 illustrates the influence of the molecular structure of the hydrocarbon on the heat flux ratio. Apparently, the structure of the hydrocarbon has little influence on the heat transfer performance of the mixture. There is insufficient data to substantiate that, in general, a branch-chain hydrocarbon will give the best heat transfer performance. Even though three different unbranched-chain hydrocarbons were tested, the data is inconclusive due to the divergence of the R123/heptane (99.5/0.5) data from the mean of the data. The molecular structure does not appear to be a primary factor in determining the influence of the additives on the R123 heat transfer performance.

Figures 25 and 26 show that neither the mole fraction nor the mass fraction have much influence on the heat transfer performance of the R123/hydrocarbon mixture. The slopes of the data appear to vary randomly from mixture to mixture. Consequently, each R123/hydrocarbon pair has a unique composition for optimum heat transfer performance.

CONCLUSIONS

The pool boiling performance of R123 on a GEWA-TTM surface was enhanced as much as (19% \pm 3%) by adding 0.5% mass isopentane. Overall, the R123/isopentane (99.5/0.5) mixture exhibited a 10 % heat transfer enhancement over the entire range of test heat fluxes. In addition, the R123/hexane (99.5/0.5) mixture showed an overall 4% and a maximum 13% heat transfer enhancement over pure R123. The pool boiling enhancement mechanism is presumably due to an accumulation of hydrocarbon at the boiling surface in the channels. Apparently, the excess layer reduces the surface-energy between the liquid and the heat transfer surface causing the production of small diameter bubbles. Smaller bubbles will induce higher site densities than larger bubbles. The site density is increased enough to more than compensate for the loss in bubble size and results in a net heat transfer enhancement.

The influence of several parameters on the pool boiling heat transfer of the R123/hydrocarbon mixtures was investigated. In general, larger heat flux ratios were obtained for R123/hydrocarbon mixtures than for hydrocarbons with smaller molecular weights. An R123/hydrocarbon mixture with a large difference in boiling points was more likely to exhibit azeotropic behavior, which led to a degradation in the heat transfer. Apparently, the structure of the hydrocarbon had little influence on the heat transfer performance of the mixture. Neither the mole fraction nor the mass fraction had much influence on the heat transfer performance of the R123/hydrocarbon mixture for the small composition range that was investigated.

ACKNOWLEDGEMENTS

This work was jointly funded by NIST and the U.S. Department of Energy (project no. DE-01-95CE23808.000 modification #A004) under Project Manager Esher Kweller. Thanks go to the following NIST personnel for their constructive criticism of the first draft of the manuscript: Dr. V. Payne, Mr. J. Gebbie, and Mrs. J. Land. The author would also like to express appreciation to

G. Glaeser and S. Nolan for data collection. Furthermore, the author extends appreciation to Dr. E. Lagergren for consultations on the uncertainty analysis.

NOMENCLATURE

English Symbols

A_s	actual surface area (m)
E_{T_w}	expanded uncertainty in the wall temperature (K)
$E_{q''}$	relative expanded uncertainty (%) in heat flux measurement
e	height of fin from tip to root (m)
k	thermal conductivity (W/m·K)
L_y	length of test surface (m)
p	exterior perimeter of test surface (m)
q''	average wall heat flux (W/m ²)
Ra_L	Rayleigh number based on A_s/p
r_c	radius of cavity mouth (m)
S_f	spacing or gap between fin-tips (m)
s	estimate of standard deviation
T	temperature (K)
T_w	temperature of surface at root of fin (K)
U	expanded uncertainty
u_i	standard uncertainty
x	test surface coordinate, Fig. 2 (m)
y	test surface coordinate, Fig. 2 (m)

Greek symbols

ΔT	wall superheat: $T_w - T_s$, (K)
σ	surface-tension (kg/s ²)

Subscripts

h	hydrocarbon
l	liquid
m	mixture
p	pure R123
s	saturated state, solid surface
v	vapor

Superscripts

-	average
---	---------

REFERENCES

- Carey, V. P., 1992, Liquid-Vapor Phase-Change Phenomena, Hemisphere, Washington.
- Cornwell, K., and Einarsson, J. G., 1989, "The Influence of Fluid Flow on Nucleate Boiling from a Tube," Eurotherm Seminar No. 8, Advances in Pool Boiling Heat Transfer, Paderborn, FRG, May 11-12, pp. 28-41.
- Belsley, D. A., Kuh, E., and Welsch, R. E., 1980, Regression Diagnostics: Identifying Influential Data and Sources of Collinearity, New York: Wiley.
- Eckert, E. R. G., and Goldstein, R. J., 1976, Measurements in Heat Transfer, Hemisphere, Washington, 2nd ed., pp. 9-11.
- Incropera, F. P., and DeWitt, D. P., 1985, Fundamentals of Heat and Mass Transfer, 2nd ed., John Wiley & Sons, New York, p. 439.
- Jontz, P. D., and Myers, J. E., 1960, "The Effect of Dynamic Surface Tension on Nucleate Boiling Coefficients," AIChE Journal, Vol. 6, No. 1. pp. 34-38.
- Kedzierski, M. A., Kim, J. H., and Didion, D. A., 1992, "Causes of the Apparent Heat Transfer Degradation for Refrigerant Mixtures," in *Two-Phase Flow and Heat Transfer*, HTD-Vol. 197, J. H. Kim, R. A. Nelson, and A. Hashemi, Eds., ASME, New York, pp. 149-158.
- Kedzierski, M. A., 1999, "Enhancement of R123 Pool Boiling by the Addition of N-Hexane," Journal of Enhanced Heat Transfer, Vol. 6, No. 4.
- Kedzierski, M. A., 1996, "Enhancement of R123 Pool Boiling by the Addition of N-Hexane," NISTIR 5780, U.S. Department of Commerce, Washington.
- Kedzierski, M. A., 1995, "Calorimetric and Visual Measurements of R123 Pool Boiling on Four Enhanced Surfaces," NISTIR 5732, U.S. Department of Commerce, Washington.
- Kedzierski, M. A., and Worthington, J. L. III, 1993, "Design and Machining of Copper Specimens with Micro Holes for Accurate Heat Transfer Measurements," Experimental Heat Transfer, Vol. 6. pp. 329-344.
- Lunger, B. S., and Shealy, G. S., 1994, "Compositions of a Hydrofluorocarbon and a Hydrocarbon," International Patent WO 94/18282.
- Morrison, G, and Ward, D. K., 1991, "Thermodynamic Properties of Two Alternative Refrigerants: 1,1-Dichloro-2,2,2-Trifluoroethane (R123) and 1,1,1,2-Tetrafluoroethane (R134a)," Fluid Phase Equilibria, Vol. 62, pp. 65-86.
- Rosen, M. J., 1978, Surfactants and Interfacial Phenomena, John Wiley & Sons, New York, p.57.

Shah, B. H., and Darby, R., 1973, "The Effect of Surfactant on Evaporative Heat Transfer in Vertical Film Flow," Int. J. Heat Mass Transfer, Vol. 16, pp. 1889-1903.

Shock, R. A. W., 1982, "Boiling in Multicomponent Fluids," Multiphase Science and Technology, Hemisphere Publishing Corp., Vol. 1, pp. 281-386.

Siu, M. C. I., Carroll, W. L., and Watson, T. W., 1976, "Thermal Conductivity and Electrical Resistivity of Six Copper-Base Alloys," NBSIR 76-1003, U.S. Department of Commerce, Washington.

Tamura, J., Tse, J. T., and Adamson, A. W., 1983, J. Japan Petrol. Inst. Vol. 26, p. 309.

Thome, J. R., 1990, Enhanced Boiling Heat Transfer, Hemisphere Publishing Corp., New York, Chap. 9.

Webb, R.L., and Pais, C., 1992, "Nucleate Pool Boiling Data for Five Refrigerants on Plain, Integral-fin and Enhanced Tube Geometries," Int. J. Heat Mass Transfer, Vol. 35, No. 8, pp. 1893-1904.

Wu, W., Yang, Y., and Maa, J., 1995, "Enhancement of Nucleate Boiling Heat Transfer and Depression of Surface Tension by Surfactant Additives," J. Heat Transfer, Vol. 117, pp. 526-529.

Table 1 Conduction model choice

Fluid	$X_0 = \text{constant (all models)}$ $X_5 = y(3x^2 - y^2)$		$X_1 = x$ $X_6 = x(3y^2 - x^2)$	$X_2 = y$ $X_7 = x^4 + y^4 - 6(x^2)y^2$	$X_3 = xy$ $X_8 = yx^3 - xy^3$	$X_4 = x^2 - y^2$
	Low q''			High q''		
R123/isopentane (99.9/0.1)	X_1, X_6, X_7 (5 of 17) 29% X_1, X_2, X_3 (4 of 17) 24% X_1, X_2 (3 of 17) 18%			X_1, X_6, X_7 (5 of 17) 29% X_1, X_2, X_3 (4 of 17) 24% X_1, X_2 (3 of 17) 18%		
R123/isopentane (99.5/0.5)	X_1 (3 of 13) 23% X_1, X_6, X_7 (2 of 13) 15%			X_1, X_3, X_6, X_7 (43 of 117) 37% X_1, X_3, X_4, X_7 (25 of 117) 21% X_1, X_5, X_6, X_7 (13 of 117) 11%		
R123/isopentane (99/1)	X_1, X_3, X_6, X_7 (25 of 64) 39% X_1, X_4, X_5, X_7 (12 of 64) 19% X_1, X_3, X_4, X_7 (6 of 64) 9%			X_1, X_3, X_6, X_7 (25 of 64) 39% X_1, X_4, X_5, X_7 (12 of 64) 19% X_1, X_3, X_4, X_7 (6 of 64) 9%		
R123/pentane (99.5/0.5)	X_1 (11 of 52) 21% X_1, X_5, X_6, X_7 (10 of 52) 19% X_1, X_6, X_7 (8 of 52) 15%			X_1 (11 of 52) 21% X_1, X_5, X_6, X_7 (10 of 52) 19% X_1, X_6, X_7 (8 of 52) 15%		
R123/pentane (99/1)	X_1 (6 of 43) 14% X_1, X_5, X_6, X_7 (6 of 43) 14% X_1, X_2, X_6, X_7 (6 of 43) 14%			X_1, X_2, X_6, X_7 (33 of 70) 47% X_1, X_2, X_4, X_7 (9 of 70) 13% X_1, X_4, X_5, X_7 (8 of 70) 11%		
R123/hexane (99.5/0.5)	X_1, X_5, X_6, X_7 (10 of 49) 20% X_1, X_3, X_6, X_7 (7 of 49) 14% X_1, X_3 (8 of 49) 16%			X_1, X_3, X_4, X_7 (30 of 118) 25% X_1, X_3, X_6, X_7 (28 of 118) 24% X_1, X_2, X_6, X_7 (28 of 118) 16%		
R123/hexane (99/1)	X_1, X_3, X_6, X_7 (26 of 110) 24% X_1, X_2, X_6, X_7 (18 of 110) 16% X_1, X_3, X_4, X_7 (17 of 110) 15%			X_1, X_3, X_6, X_7 (26 of 110) 24% X_1, X_2, X_6, X_7 (18 of 110) 16% X_1, X_3, X_4, X_7 (17 of 110) 15%		
R123/heptane (99.5/0.5)	X_1 (12 of 33) 36% X_1, X_3 (9 of 33) 27% X_1, X_6, X_7 (4 of 33) 12%			X_1, X_3, X_6, X_7 (47 of 78) 60% X_1, X_3, X_4, X_7 (27 of 78) 35% X_1, X_2, X_4, X_7 (2 of 78) 3%		
R123/cyclohexane (99.5/0.5)	X_1, X_2, X_3 (11 of 38) 29% X_1, X_2, X_3, X_6 (5 of 38) 13% X_1, X_2, X_4, X_5 (4 of 38) 11%			X_1, X_3, X_6, X_7 (43 of 181) 24% X_1, X_4, X_5, X_7 (34 of 181) 19% X_1, X_2, X_4, X_7 (14 of 181) 8%		
R123/cyclohexane (99/1)	X_1, X_3, X_6, X_7 (38 of 124) 31% X_1, X_3, X_4, X_7 (23 of 124) 19% X_1, X_3, X_4, X_6 (9 of 124) 7%			X_1, X_3, X_6, X_7 (38 of 124) 31% X_1, X_3, X_4, X_7 (23 of 124) 19% X_1, X_3, X_4, X_6 (9 of 124) 7%		
R123	X_1, X_5, X_6, X_7 (23 of 66) 35% X_1, X_6, X_7 (14 of 66) 21% X_1, X_3, X_6, X_7 (7 of 66) 11%			X_1, X_3, X_6, X_7 (57 of 210) 27% X_1, X_3, X_4, X_7 (52 of 210) 25% X_1, X_2, X_6, X_7 (34 of 210) 16%		

Table 2 Pool boiling data

R123/hexane
(99.5/0.5)

File:
GT5HEX.DAT

$\Delta T_s(K)$	$q'' (W/m^2)$
10.604	76976.3
10.623	76334.3
10.611	76623.8
10.529	68496.7
10.519	68946.4
10.347	58373.2
10.398	55786.1
10.383	55593.8
10.113	47180.3
10.092	46989.9
10.016	42193.1
10.000	41713.3
10.004	42045.1
9.933	38958.1
9.897	38522.3
9.894	39932.8
9.653	30721.0
9.627	31256.0
9.666	30995.2
9.292	25087.9
9.287	24930.5
9.316	25257.3
9.136	24815.3
8.465	20630.1
8.574	20612.2
8.560	20257.6
10.604	75278.3
10.587	75395.3
10.586	74754.7
10.428	61473.8
10.433	61547.8
10.420	61182.4
10.328	51877.0
10.265	53048.0
10.252	53354.3
10.090	44646.0
10.000	41778.8
9.993	42878.2
9.907	39062.6
9.893	39467.7
9.884	39140.8
9.754	34072.1
9.751	34446.7
9.755	34102.5
9.494	28812.5
9.512	28807.3
9.493	29981.7
8.779	23280.0
8.740	23024.0
8.740	23339.3
8.023	17927.2
7.900	17413.7
7.942	17746.7
6.492	14171.2
6.428	13836.7
6.462	14062.6
3.218	4741.1
3.160	4574.3
3.117	4420.8
10.654	75388.5
10.617	75022.5
10.591	75015.2
10.539	69794.5
10.529	69862.0
10.516	69863.8
10.467	64970.8
10.465	65699.3
10.457	66477.8
10.343	59049.8
10.364	59818.4
10.365	59466.4
10.196	54406.1
10.185	53758.2
10.182	53198.0
9.986	44074.9
9.962	44109.0
9.935	43432.2
9.778	35491.8
9.808	35864.8
9.698	36474.9
9.199	27075.3
9.183	27380.7
9.256	26730.7
8.132	19483.4
8.148	19796.7
8.145	20281.5
6.933	14662.9
7.017	14157.8
7.066	14853.1
6.121	13214.8
6.072	12567.3

10.570	76641.4
10.578	78231.7
10.580	77518.1
10.547	74399.2
10.534	73565.2
10.480	68138.2
10.518	70904.3
10.466	67804.6
10.434	67040.6
10.371	62251.6
10.331	62257.4
10.319	59935.1
10.302	58019.1
10.304	57738.0
10.224	59335.5
9.808	49379.3
9.637	46088.8
9.719	44248.0
9.793	41833.5
9.700	40135.5
9.692	39575.4
9.674	39495.1
9.436	31964.9
9.486	32283.2
9.459	32134.6
8.864	25410.7
9.042	27275.5
9.074	27578.6
8.251	18885.6
8.172	18909.1
8.137	18794.3
6.436	13780.7
6.439	13333.7
6.451	13317.0
10.570	76641.4
10.578	78231.7
10.580	77518.1
10.547	74399.2
10.534	73565.2
10.480	68138.2
10.518	70904.3
10.466	67804.6
10.434	67040.6
10.371	62251.6
10.331	62257.4
10.319	59935.1
10.302	58019.1
10.304	57738.0
10.224	59335.5
9.808	49379.3
9.637	46088.8
9.719	44248.0
9.793	41833.5
9.700	40135.5
9.692	39575.4
9.674	39495.1
9.436	31964.9
9.486	32283.2
9.459	32134.6
8.864	25410.7
9.042	27275.5
9.074	27578.6
8.251	18885.6
8.172	18909.1
8.137	18794.3
6.436	13780.7
6.439	13333.7
6.451	13317.0

R123/hexane
(99/1)

File:
GT1HEX.DAT

$\Delta T_s(K)$	$q'' (W/m^2)$
10.553	77774.6
10.551	78431.4
10.530	78414.9
10.375	66238.7
10.395	66251.5
10.422	65607.0
10.234	53851.8
10.246	55155.3
10.074	50199.5
10.081	49493.8
10.065	49586.0
9.894	41126.4
9.952	40847.0
9.958	41037.6
9.604	29616.5
9.577	29920.3
9.603	29965.7
8.970	28136.4
9.031	28909.5
9.047	28883.2
8.698	24410.9
8.732	24581.7

8.739	25025.1
10.657	76769.9
10.653	77234.8
10.656	77431.6
10.524	67745.2
10.521	67894.2
10.542	66350.9
10.457	62293.3
10.311	62380.7
10.163	57384.6
10.145	56287.0
10.136	56764.3
10.040	49699.5
10.053	50314.1
10.062	50544.9
9.897	40455.2
9.860	41080.5
9.848	40526.7
9.608	34808.9
9.708	35738.3
9.697	35456.3
9.405	30391.4
9.417	29306.2
9.336	33405.9
9.186	28170.0
9.178	31159.7
9.239	28362.7
9.084	26940.8
9.114	26956.9
9.109	29516.6
8.628	19741.4
8.656	20007.6
8.684	20197.8
10.742	79637.5
10.742	80608.5
10.714	80823.2
10.590	72530.6
10.583	72218.0
10.566	71926.0
10.406	59150.6
10.378	57970.8
10.381	59198.7
10.375	54836.2
10.388	54898.4
10.380	54458.3
10.072	42847.9
10.116	46297.3
10.202	47098.5
9.879	36282.0
9.828	35758.8
9.858	36791.0
9.224	24883.6
9.705	32403.7
9.131	27042.4
9.404	29092.7
9.492	29880.5
9.156	27006.1
9.106	28638.3
8.811	22358.2
8.637	20958.0
8.223	18572.6
8.230	18205.8
8.222	18094.9
7.609	15366.9
7.568	16978.9
10.665	76535.9
10.636	75091.3
10.468	63677.5
10.446	63049.2
10.457	63959.6
10.370	57308.0
10.382	57606.8
10.286	52592.0
10.284	52486.2
10.074	46388.7
10.074	46640.8
10.052	46052.8
9.883	38605.0
9.848	38708.5
9.811	38785.3
9.600	31827.0
9.569	32564.2
9.604	31441.4
8.978	28224.2
9.047	28509.5
9.109	25960.1
8.872	26573.8
8.895	27067.1
10.664	75556.7
10.689	75195.5
10.478	62722.5
10.470	63416.2
10.466	63663.3
10.477	63231.6
9.765	35107.0
10.354	55564.5
10.147	47799.4
10.145	48708.4
10.114	48076.3
9.799	35141.6

9.770	35075.1
9.563	29471.4
9.560	29997.0
9.567	30191.8
8.983	27705.0
8.992	26041.7
8.680	21257.7
8.645	23278.6
8.669	21631.0
7.701	15876.2
7.681	15840.2
7.698	15593.3
6.152	10927.9
6.085	12517.2
6.058	11953.4
10.649	75537.2
10.670	77683.7
10.651	77426.8
10.573	70097.6
10.567	69973.5
10.573	70444.8
10.433	62357.0
10.432	62290.6
10.406	61760.1
10.383	58079.8
10.368	58048.6
10.370	58455.2
10.025	45078.1
10.048	46033.3
10.057	46645.7
9.884	40089.1
9.881	40019.9
9.845	40327.2
9.552	29680.9
9.500	31137.1
9.554	30300.0
8.741	26801.8
8.754	25030.5
8.758	26630.3
8.784	26480.1
8.766	26027.0
8.747	25919.4
8.698	22920.2
8.689	23038.0
8.698	23453.7
8.435	19934.3
8.406	19199.2
8.410	19202.6
7.925	16540.4
7.868	16252.9
7.881	16346.5
7.355	14462.7
7.203	15408.3

R123/isopentane
(99.5/0.5)

File:
GT5ISO.DAT

$\Delta T_s(K)$	$q'' (W/m^2)$
10.654	84348.5
10.640	84665.0
10.638	85543.1
10.452	73786.4
10.427	73821.7
10.426	73631.0
10.246	64881.1
10.201	64339.2
10.195	63898.0
10.007	51668.5
9.944	53399.3
9.978	52060.0
9.795	43693.3
9.746	42537.3
9.737	42639.0
9.551	35643.9
9.559	35777.2
9.212	27765.1
9.269	27780.2
9.295	27810.5
9.536	39822.1
10.528	72520.0
10.504	73490.4
10.483	74834.1
10.355	64328.4
10.341	64042.6
10.361	64209.2
10.222	54201.9
10.200	53731.5
10.127	52876.0
9.929	49219.3
9.985	51791.7
9.979	51940.0
9.779	41799.5
9.780	41430.5

9.784	41637.8
9.583	33724.6
9.529	34904.6
9.531	34502.4
9.565	32421.6
9.515	32173.3
9.501	31459.9
8.937	23012.7
8.916	22590.1
6.164	10296.3
6.147	10606.9
6.109	10469.0
10.559	76942.2
10.540	77670.1
10.631	78227.5
10.456	68565.1
10.417	68709.4
10.414	67924.5
10.284	59693.2
10.238	58544.5
10.224	59185.7
10.120	48718.9
10.129	48177.6
10.123	48521.4
10.000	42248.0
9.930	44169.8
9.966	42429.2
9.706	33561.6
9.692	33940.3
9.685	34462.4
9.303	25548.9
9.313	25739.0
9.267	25701.1
9.027	24210.0
9.004	24808.9
9.016	24109.8
8.401	18583.8
8.429	18796.2
8.429	18899.4
3.392	3678.8
3.379	3860.0
3.552	4688.1
10.528	80876.3
10.538	84209.2
10.577	84774.8
10.287	62766.7
10.254	61362.0
10.190	54975.4
10.168	55133.9
10.134	55362.4
9.929	47478.2
9.926	46878.6

File:
GT1ISO.DAT

ΔT_i (K)	α^* (W/m ²)
10.352	71133.9
10.354	70977.8
10.365	70357.8
10.287	62609.9
10.308	62244.9
10.320	62325.0
10.228	57487.2
10.233	57989.1
10.228	57490.6
10.175	52879.2
10.164	54135.8
10.163	54175.3
10.015	50071.3
10.039	50343.4
10.022	47730.2
9.796	42607.6
9.823	43213.5
9.760	38097.8
9.782	38176.7
9.790	38190.3
9.569	33099.9
9.602	31847.5
9.614	32446.7
9.446	29197.2
9.426	29083.5
9.428	29294.8
9.305	25883.7
9.320	24726.5
9.327	25091.9
9.235	23449.8
9.207	23752.3
9.240	23692.8
10.459	72382.4
10.488	74603.4
10.492	76190.3
10.451	73153.6
10.452	74738.3
10.427	74431.3
10.299	64095.1
10.276	64317.1
10.281	63856.4
10.161	56018.4
10.194	57432.1
10.179	58581.3
10.082	50338.1
10.083	50182.6
10.083	50182.6
9.884	40452.7
9.861	42031.2
9.839	42120.2
9.703	34202.9
9.690	34535.4
9.692	34394.9
9.529	31597.1
9.496	31542.6
9.514	31541.1
8.965	27338.6
9.049	26906.6
8.749	24366.6
8.711	23708.2
8.669	23276.4
7.865	18765.7
7.965	20086.0
7.989	19927.2

R123/isopentane
(99.9/0.1)

File:
GT01ISO.DAT

ΔT_i (K)	α^* (W/m ²)
10.784	75064.9
10.767	75491.0
10.759	76299.8
10.640	65597.2
10.619	65959.5
10.611	65900.3
10.517	57560.4
10.507	57447.0
10.447	56734.4
10.307	48342.1
10.351	49184.7
10.022	38453.5
10.021	38945.9
10.001	38691.2
9.757	31696.3
9.642	33268.7
9.658	32474.0
9.724	33584.7
9.345	27583.7
9.364	27692.2
9.343	27406.7
8.697	22064.7
8.693	23388.2
8.698	23636.9
7.800	15469.0

7.765	17342.8
7.780	17362.5
7.238	15016.7
7.159	14851.8
7.171	14856.7
10.784	75064.9
10.767	75491.0
10.759	76299.8
10.640	65597.2
10.619	65959.5
10.611	65900.3
10.517	57560.4
10.507	57447.0
10.447	56734.4
10.307	48342.1
10.351	49184.7
10.022	38453.5
10.021	38945.9
10.001	38691.2
9.757	31696.3
9.642	33268.7
9.658	32474.0
9.724	33584.7
9.345	27583.7
9.364	27692.2
9.343	27406.7
8.697	22064.7
8.693	23388.2
8.698	23636.9
7.800	15469.0
7.765	17342.8
7.780	17362.5
7.238	15016.7
7.159	14851.8
7.171	14856.7
10.726	73987.5
10.738	74282.6
10.659	69019.0
10.630	69208.8
10.634	68756.2
10.577	65174.1
10.574	65379.7
10.561	65843.2
10.354	54739.5
10.269	55914.8
10.285	56701.2
10.146	48345.4
10.060	44931.6
10.057	45114.2
10.054	45817.2
9.561	32379.2
9.580	32742.6
9.585	32781.4
8.913	27097.3
8.921	25213.2
8.913	27553.8
8.369	21284.2
8.402	18728.8
10.845	75358.4
10.725	75891.4
10.650	75832.8
10.662	78035.7
10.567	73119.9
10.579	73173.7
10.558	72916.0
10.434	60107.0
10.411	59834.2
10.423	60248.8
10.341	56839.5
10.342	56424.9
10.350	56190.0
10.267	54584.4
10.254	54644.0
10.262	54368.4
10.153	50789.5
10.037	51396.0
9.947	47830.0
9.972	48394.3
10.049	47463.7
9.808	42972.5
9.809	43061.2
9.833	43637.6
9.300	32040.6
9.266	31911.1
9.274	30343.1
9.730	20178.8
7.911	19281.0
7.908	17703.7
10.670	73622.6
10.664	73694.8
10.643	74076.7
10.635	70144.1
10.633	69749.1
10.643	70103.0
10.429	60384.4
10.431	60419.2
10.398	59624.3
10.338	55133.0
10.326	55896.1
10.315	55874.6
9.976	46949.0
9.967	47080.6

R123/cyclohexane
(99/1)

File:
GT1CYC.DAT

ΔT_i (K)	α^* (W/m ²)
11.111	73931.5
11.104	74433.5
11.109	74214.3
10.999	61268.9
10.891	63279.4
10.880	63596.2
10.698	51435.6
10.719	51685.2
10.520	43234.2
10.483	43106.8
10.513	43118.7
10.517	43395.2
10.093	35239.6
10.079	35348.9
9.378	29113.8
9.179	30040.6
9.186	29446.3
8.595	25827.3
8.631	24404.8
8.652	24281.4
8.752	23204.8
8.669	22277.0
7.446	16243.3
7.432	16333.9
7.464	16874.4
6.814	14341.8
6.750	13640.9
6.750	13683.9
11.052	72977.7
11.028	72986.1
10.993	73500.7
10.870	61429.0
10.868	62990.8

10.864	62937.3
10.839	58121.0
10.811	57763.6
10.798	57966.7
10.737	54876.1
10.731	54279.6
10.679	51612.3
10.435	43853.9
10.401	43976.2
10.395	46224.5
10.168	37219.5
10.181	37183.8
10.098	36013.9
10.072	36433.3
10.099	36684.9
10.112	36468.9
9.784	30043.0
9.773	29914.4
9.763	29875.2
9.325	29422.4
9.351	29854.5
8.918	24778.9
8.919	24829.9
8.077	19621.8
8.233	18172.0
11.019	75287.3
11.018	75526.1
10.999	75553.5
10.939	72850.1
10.766	61456.5
10.746	62594.3
10.323	44437.2
10.308	43805.8
9.907	32811.2
9.953	33215.1
9.941	33256.8
9.051	24923.8
9.106	25346.3
8.970	22080.0
9.007	22367.5
8.913	23962.0
11.034	72713.3
11.034	72713.3
10.985	72498.7
10.958	71991.8
10.915	68456.1
10.883	68229.0
10.870	67813.6
10.753	63238.5
10.652	54786.4
10.668	56402.0
10.681	56147.3
10.558	52148.9
10.543	52429.4
10.573	52595.4
9.956	35129.9
10.079	34126.7
10.048	34802.8
9.609	28788.1
8.902	24190.0
8.911	23940.7
8.902	24142.6
7.772	16408.5
7.613	15951.8
7.595	16553.6
10.825	72928.5
10.997	78735.3
11.021	78846.7
10.848	71970.1
10.764	65598.4
10.654	59809.9
10.595	61058.2
10.561	60232.0
10.274	47316.7
10.263	47349.1
10.239	46464.3
10.131	42414.5
10.129	43668.3
10.151	44115.3
10.062	40621.1
9.852	36268.6
9.909	37081.8
9.924	37231.2
9.366	29054.2
9.361	29366.2
9.365	29224.1
9.139	25408.1
9.096	25090.0
9.092	25107.1
8.453	22173.6
8.460	22113.1
10.980	71766.3
10.984	71411.4
10.997	71826.8
10.965	67577.9
10.991	67793.3
10.943	68634.2
10.731	56275.7
10.706	56832.6
10.488	47339.9
10.496	47381.5
10.495	46853.0

R123/cyclohexane
(99.5/0.5)

File:
GT5CYC.DAT

ΔT_i (K)	α^* (W/m ²)
10.843	76946.0
10.821	76481.4
10.828	75826.2
10.665	64437.5
10.672	68411.3
10.611	59630.0
10.611	59578.6
10.590	59302.7
10.451	51263.3
10.461	49088.2
10.468	49158.8
10.369	48643.2
10.363	48640.4
10.337	48058.2
10.385	42464.6
10.142	39633.0
10.185	40402.0
10.168	37460.3
10.174	37320.8
10.172	37359.1
9.867	29886.2
9.805	29907.5
9.720	27900.5
9.588	26242.9
9.699	26317.2
9.649	26549.1
8.958	22144.9
9.013	21480.8
9.033	21296.6
7.682	15217.6
7.793	17385.6
7.901	16260.3
6.741	12774.7
6.743	13579.6
6.758	12584.5
5.845	11620.8
5.814	11445.9
5.830	11454.9
10.796	77335.4
10.826	77004.0
10.837	77177.9
10.708	69097.6
10.697	67469.0
10.672	67513.0
10.638	64991.5

10.636
10.637
10.586
10.572
10.513
10.464
10.424
10.383
10.304
10.291
10.287
10.008
9.975
9.998
9.525
9.482
9.206
9.039
9.075
8.652
8.704
8.676
8.453
8.359
8.403
6.506
6.520
6.576
10.773
10.749
10.758
10.685
10.690
10.686
10.662
10.618
10.602
10.601
10.452
10.431
10.405
10.298
10.312
10.305
10.236
10.239
10.246
10.121
9.988
9.942
9.253
9.263
9.259
11.079
10.978
10.944
10.805
10.745
10.783
10.623
10.585
10.504
10.483
10.293
10.305
10.301
9.481
9.510
9.563
10.908
10.877
10.897
10.809
10.806
10.787
10.739
10.739
10.730
10.475
10.504
10.525
10.409
10.406
10.415
10.283
10.282
10.276
10.047
10.005
9.978
9.451
9.415
9.343
9.380
9.374
8.775
8.737
8.725
7.954
8.020
8.011
10.920

65833.4
66334.5
58678.1
56250.3
57677.0
50565.6
48328.5
51138.3
46753.4
46954.7
46596.9
34468.6
34410.7
33823.9
25780.3
25461.0
24545.0
23899.6
24279.5
22818.5
22166.8
22486.6
19270.4
20773.6
20816.7
13298.8
13287.5
13340.6
74484.0
72259.4
75320.7
65898.5
66033.3
64801.7
59741.6
59501.1
60409.5
56648.2
49822.4
49130.6
47988.8
41881.2
44029.1
44707.4
40406.8
39927.7
40099.6
34616.8
34660.5
33644.3
26161.4
25772.7
26310.2
73184.5
71583.3
71696.6
59297.2
60150.4
58882.0
53204.4
52828.2
43764.6
44107.6
35377.8
36062.1
36227.8
27201.2
24579.0
24807.1
75512.6
75484.3
75144.2
66702.0
66650.2
66561.0
62915.9
62563.6
62253.3
51054.9
51292.7
51352.6
46063.0
45871.7
46551.3
40205.1
41321.0
40487.6
32725.6
32297.9
32298.2
26971.0
26625.1
25885.5
26111.9
26030.6
19639.9
19507.2
20278.4
16308.2
16386.4
16425.0
74408.6

R123/pentane
(99.5/0.5)
File:
GT5PEN.DAT

ΔT (K)	q^* (W/m ²)
10.530	77189.0
10.507	78270.7
10.531	78851.2
10.429	65946.5
10.440	65960.0
10.437	65402.3
10.311	51040.0
10.296	52760.9
10.352	55911.6
10.242	51735.6
10.238	51987.8
10.281	50154.4
10.113	44644.2
10.116	43849.3
10.140	45196.8
10.074	42984.1
10.074	42021.2
10.099	42167.6
10.005	36777.8
9.992	37931.3
9.976	38756.1
9.905	31528.8
9.939	31656.4
9.935	31816.9
9.772	28344.5
9.746	27753.0
9.684	26931.0
9.113	25133.2
9.142	25503.5
9.301	23343.2
8.636	21465.8
8.684	21550.9
8.647	21461.4
7.772	16793.9
7.823	16919.3
7.810	16359.4
10.638	77573.0
10.616	76419.1
10.593	75982.9
10.509	70652.4
10.496	70330.0
10.500	69908.5
10.420	60903.2
10.447	60664.5
10.445	60638.3
10.399	57382.0
10.408	57521.6
10.288	46924.1
10.266	46827.2
10.269	46581.0
9.995	34052.0
10.047	34344.9
9.708	26596.8
9.646	27419.1
9.646	26194.2
9.330	25167.9

R123/pentane
(99/1)
File:
GT1PEN.DAT

ΔT (K)	q^* (W/m ²)
10.502	73285.6
10.502	74053.8
10.498	74377.8
10.449	70012.9
10.433	69793.3
10.409	69856.1
10.376	66951.8
10.376	66481.8
10.328	58297.6
10.319	57767.5
10.320	58181.2
10.175	50357.5
10.211	48983.3
10.176	48930.5
10.017	40398.2
10.026	40650.3
10.037	40243.2
9.696	28206.6
9.491	29343.0
9.423	29293.3
9.398	27590.0
9.455	26020.7
9.464	26466.6
8.956	22535.2
9.011	22217.1
8.962	22600.4
8.578	20890.9
8.601	21286.8
8.652	21565.4
7.808	19818.3
7.853	19398.3
7.808	19480.7
10.602	69724.9
10.604	71458.9
10.573	71126.0

27545.1
26191.0
18726.0
18768.4
19215.9
13429.8
13439.0
13407.7
12348.1
13805.2
12091.4
11103.0
11336.2
11118.6
10170.3
10264.4
8660.2
8592.6
8609.4
6937.5
6915.5
6853.6
74426.3
74765.2
75207.8
72777.0
72351.7
72495.1
65423.9
65483.8
64218.6
47201.2
47038.6
47383.7
39890.6
39785.7
40329.4
27314.2
27264.6
27626.5
26033.8
26186.6
24346.3
21011.1
20875.5
21121.9
19282.4
19331.1
15784.9
16022.2
16159.7
14074.0
13969.4
13955.2
10568.5
11340.8
11488.4

10.572
10.573
10.590
10.539
10.539
10.518
10.521
10.469
10.549
10.515
10.512
10.433
10.451
10.434
10.365
10.354
10.366
10.235
10.184
10.246
10.111
10.153
10.091
9.969
9.922
9.915
9.543
9.339
9.282
8.279
8.332
8.286
7.711
7.704
7.560
7.097
7.183
7.255
6.583
6.612
6.550
5.734
5.694
5.580
4.591
4.556
4.570
10.441
10.450
10.334
10.300
10.299
10.125
10.091
10.110
10.000
9.975
9.981
9.793
9.799
9.796
8.806
8.831
8.836
8.073
8.039
8.062
6.540
6.497
6.481
5.983
5.896
5.480
5.477
5.128
5.210
4.418
4.448

R123/heptane
(99.5/0.5)
File:
GT5SHEP.DAT

ΔT (K)	q^* (W/m ²)
11.327	72301.820
11.319	72641.780
11.329	72095.440
11.156	63700.860
11.154	64383.910
11.138	64027.380
10.933	55020.690
10.915	55033.350
10.917	54875.680
11.247	72188.070
11.260	72218.030
11.184	71863.290
11.025	63988.800
11.072	64512.120
11.142	64019.050
11.006	55917.680

69453.0
69418.7
69565.7
66985.0
66985.0
67281.8
66950.2
59108.2
71151.1
68719.6
70836.1
65771.5
65459.6
65215.2
57120.8
56416.4
56885.0
49449.2
50803.4
52638.6
45351.0
43431.7
45560.7
33820.4
33956.5
35022.5
26608.9
27086.7
26973.0
19779.7
18935.4
19489.5
17895.6
17286.2
17017.9
15874.4
16058.6
16214.1
16049.0
15928.3
16078.1
13160.1
13039.3
12579.6
9225.9
9401.8
9381.3
73523.3
73384.3
63502.7
63763.8
64051.4
48977.3
48079.3
46371.3
41144.6
40258.7
40617.5
31853.1
31918.4
32009.4
21992.3
22223.6
22335.8
18550.5
20590.3
18380.8
15533.0
15372.4
15174.0
13448.8
13359.9
11946.2
11956.9
10731.4
11075.9
8324.1
8471.7

11.018
11.013
10.892
10.886
10.879
10.635
10.627
10.647
10.328
10.325
10.330
9.747
9.789
9.766
8.923
8.901
8.951
8.462
8.394
8.386
7.976
7.896
7.891
11.224
11.267
11.277
11.148
11.158
11.157
10.988
10.961
10.960
10.744
10.716
11.382
11.389
11.368
11.271
11.279
11.258
11.208
11.180
11.158
10.970
10.981
11.047
10.693
10.756
10.749
10.548
10.579
10.554
10.451
10.449
10.228
10.245
9.466
9.391
9.418
8.609
8.566
8.574
7.275
7.245
7.198
11.380
11.461
11.441
11.247
11.225
11.220
11.137
11.127
11.121
10.826
10.821
10.823
10.508
10.495
10.028
10.063
10.050
9.249
9.274
9.318
8.979
9.019
8.944
7.836
7.821
7.803
7.202
7.161
7.123

R123
File:
GTFLDN.DAT

56155.390
56328.840
46680.610
48265.960
47013.360
38852.760
38025.290
38412.350
32643.710
32628.020
32425.280
29851.740
29929.970
29776.100
20076.290
21954.960
21850.880
17146.950
18648.020
16803.040
16675.900
16607.490
16583.510
76471.270
78175.070
78373.330
70748.320
70006.630
70063.700
60124.870
60416.020
61120.050
51919.240
54290.720
72288.230
72199.000
71840.170
64778.450
64959.540
64419.360
60118.720
60021.780
60044.410
53194.990
53752.540
53548.300
42139.690
42028.090
42120.740
34996.520
35532.950
35663.320
33308.550
33240.300
32831.390
30857.720
31168.600
25534.810
25713.020
25642.390
19153.960
19518.790
19426.800
14814.380
14792.260
14791.260
73828.450
77214.940
77833.630
66935.390
66874.650
66113.950
59114.020
58760.120
59234.130
47345.450
47688.610
48001.470
36595.680
37150.810
29469.170
30036.540
30171.050
22354.330
22194.410
22598.170
20441.540
19213.640
21603.390
15999.110
15969.800
15912.550
13899.690
13709.550
13585.680

ΔT_s (K)	q'' (W/m ²)								
10.562	67849.5	9.158	24179.2	10.300	58432.3	10.491	64191.4	6.883	14027.3
10.546	70318.8	9.156	24096.8	10.081	50168.7	10.483	65151.8	6.765	13837.5
10.561	71190.3	9.161	24017.4	10.074	49677.1	10.388	55387.8	6.343	12681.1
10.505	65318.1	8.929	22063.2	10.074	49137.4	10.045	42880.3	6.423	12911.0
10.508	65563.0	8.918	21575.1	9.944	45286.3	10.112	46439.6	6.434	12901.3
10.489	65156.7	8.894	21962.9	9.925	45755.5	10.118	46352.3	5.723	11899.1
10.489	65156.7	10.642	74716.6	9.812	39678.3	9.990	40012.9	5.712	12018.3
10.429	58931.7	10.623	70798.8	9.803	39001.8	9.969	40055.1	5.718	12026.0
10.409	58934.5	10.602	71507.4	9.785	39460.0	9.935	37859.0	4.375	7998.6
10.406	58386.5	10.462	66053.5	9.653	30847.9	9.900	35900.8	4.319	7813.2
10.326	53430.4	10.546	70273.5	9.686	30830.0	9.905	35920.9	4.281	7743.2
10.319	53752.0	10.428	62980.0	9.666	31686.0	9.876	36314.4	10.463	74774.7
10.300	54158.8	10.403	62697.5	9.056	26719.1	9.643	30427.1	10.473	75628.3
10.156	50168.9	10.447	62857.3	9.057	26718.3	9.705	31029.8	10.476	75465.2
10.135	50253.9	10.357	55542.4	9.056	26923.7	9.603	28908.2	10.384	66881.8
9.916	39976.9	10.367	55176.5	8.103	20275.1	9.520	27983.9	10.379	67125.3
9.896	39837.1	10.229	55344.2	8.071	20061.4	9.526	27825.1	10.393	66602.5
9.900	39847.7	10.293	53744.1	10.565	74084.1	9.551	28000.5	10.309	58291.4
9.723	36242.7	10.170	46021.4	10.557	75398.2	9.370	29502.0	10.293	58641.1
9.740	35292.3	10.148	46255.9	10.576	77791.3	9.043	24847.9	10.155	53543.8
9.773	34923.3	10.125	46441.7	10.515	73731.3	9.031	23706.9	10.114	54085.5
9.527	30650.9	9.979	38281.9	10.536	73678.8	8.354	18301.1	10.127	53223.4
9.538	30498.3	9.993	39569.9	10.531	74241.4	8.418	18471.5	9.994	45418.1
9.584	29118.1	9.998	40472.2	10.393	61736.4	8.277	17623.9	9.978	44951.6
9.212	25495.8	9.906	37435.4	10.378	61166.2	6.601	12776.5	9.959	45357.5
9.133	26361.7	9.893	38141.4	10.361	58207.8	6.624	14208.8	9.827	37097.5
10.571	73581.9	9.903	37328.9	10.321	52763.1	10.533	76637.2	9.823	36973.2
10.614	77143.4	9.651	28001.7	10.319	54585.8	10.556	78693.5	9.825	37229.2
10.607	78115.3	9.625	28800.6	10.315	55210.8	10.558	79748.9	9.461	32987.3
10.546	70964.8	9.657	29526.1	10.170	45571.4	10.481	66709.8	9.401	32973.3
10.570	71110.9	9.341	28251.3	10.093	46878.7	10.427	66373.5	9.397	32954.7
10.566	71008.0	9.281	28307.2	10.103	47341.5	10.417	66810.2	9.021	28075.7
10.492	66332.9	9.335	28912.1	9.944	41402.8	10.337	60987.2	8.941	28929.1
10.479	64730.9	9.068	24843.4	9.923	40718.2	10.337	60987.2	9.027	28134.1
10.450	61133.5	9.092	24625.0	9.893	38389.6	10.317	60698.0	8.953	28435.7
10.440	61369.3	9.134	25838.8	9.706	32526.5	10.322	62050.1	8.985	29839.6
10.455	61404.8	8.843	20998.5	9.696	31833.2	10.175	52777.2	9.052	27365.1
10.353	55113.7	8.853	20823.9	9.683	31840.0	10.184	53010.0	8.681	22594.9
10.330	55318.9	8.877	20682.1	9.574	29407.7	9.643	30427.1	8.661	22203.5
10.229	50709.0	8.501	18113.7	9.568	29434.1	10.190	52692.8	8.667	22672.1
10.200	50517.5	8.492	18058.8	9.450	30199.6	10.024	44457.7	7.698	18765.2
10.180	50816.0	8.499	18269.6	9.566	29404.9	9.991	43808.8	7.689	16734.8
10.112	45722.6	7.719	16956.2	9.027	27884.4	9.972	43968.4	7.778	17493.6
10.103	45885.5	7.787	15367.2	9.012	27862.7	9.808	34897.2	6.968	16129.8
10.074	45283.7	7.756	17268.7	8.796	26061.9	9.813	35012.8	7.016	16186.8
10.023	41985.6	7.187	13632.1	8.892	25278.4	9.282	30843.2	7.032	16309.8
9.972	40758.1	7.203	13612.2	8.930	25325.2	9.293	30908.6	5.867	12457.8
9.812	32430.1	7.175	15473.3	8.800	23815.7	9.296	31056.1	5.835	10784.8
9.806	33109.5	10.615	77166.7	8.840	24609.7	8.592	20948.7	5.833	12556.9
9.811	33397.9	10.602	76991.8	8.867	23881.9	8.579	20811.7		
9.597	28139.9	10.596	76544.6	7.456	15254.3	8.563	20881.6		
9.524	30884.5	10.596	76544.6	7.402	15028.8	8.398	19940.7		
9.587	29191.0	10.436	64851.8	7.367	15098.4	8.421	20336.4		
9.312	28945.9	10.392	64890.2	10.615	76070.2	7.257	15064.2		
9.338	28862.6	10.336	65476.0	10.636	77280.7	7.222	15144.9		
9.346	28760.1	10.304	57889.6	10.641	77489.4	7.209	15407.7		
		10.306	58126.3	10.489	68287.0	6.903	13952.7		

Table 3 Number of test days and data points

Fluid (% mass)	Number of days	Number of data points
R123/isopentane (99.9/0.1)	7	186
R123/isopentane (99.5/0.5)	5	130
R123/isopentane (99/1)	2	64
R123/pentane (99.5/0.5)	3	113
R123/pentane (99/1)	4	113
R123/hexane (99.5/0.5)	5	158
R123/hexane (99/1)	6	175
R123/heptane (99.5/0.5)	5	111
R123/cyclohexane (99.5/0.5)	6	177
R123/cyclohexane (99/1)	7	182
R123	8	276

Table 4 Constants for cubic boiling curve fits for GEWA-T™

$$\Delta T_s = A_0 + A_1 q'' + A_2 q''^2 + A_3 q''^3$$

ΔT_s in Kelvins and q'' in W/m^2

Fluid		A_0	A_1	A_2	A_3
R123/isopentane (99.9/0.1)	$\Delta T_s \geq 8.5K$	5.162564	2.213069×10^{-4}	-3.305539×10^{-9}	1.794215×10^{-14}
	$\Delta T_s \leq 9.5K$	3.242045	2.982389×10^{-4}	$-9.070653 \times 10^{-10}$	-7.87954×10^{-14}
R123/isopentane (99.5/0.5)	$\Delta T_s \geq 8K$	6.596237	1.387433×10^{-4}	-1.89345×10^{-9}	9.752913×10^{-15}
	$\Delta T_s \leq 9.5K$	-1.953420	1.143663×10^{-3}	-4.152663×10^{-8}	5.346848×10^{-13}
R123/isopentane (99/1)	$\Delta T_s \geq 0K$	6.239937	1.715029×10^{-4}	-2.614962×10^{-9}	1.441917×10^{-14}
	$\Delta T_s \leq 10K$	-5.436468	1.228280×10^{-3}	-3.369096×10^{-8}	3.120554×10^{-13}
R123/pentane (99.5/0.5)	$\Delta T_s \geq 9.7K$	8.725847	5.269372×10^{-5}	$-5.821089 \times 10^{-10}$	2.857575×10^{-15}
	$\Delta T_s \leq 9.7K$	9.454738×10^{-1}	4.434199×10^{-4}	-1.626985×10^{-9}	$-1.148459 \times 10^{-13}$
R123/pentane (99/1)	$\Delta T_s \geq 9K$	6.665111	1.609068×10^{-4}	-2.494825×10^{-9}	1.396698×10^{-14}
	$\Delta T_s \leq 9K$	5.494870	-5.514591×10^{-4}	6.175966×10^{-8}	$-1.360361 \times 10^{-12}$
R123/hexane (99.5/0.5)	$\Delta T_s \geq 9K$	7.052807	1.128998×10^{-4}	-1.337031×10^{-9}	6.112061×10^{-15}
	$\Delta T_s \leq 9K$	2.307429	7.110618×10^{-5}	2.923709×10^{-8}	$-8.785910 \times 10^{-13}$
R123/hexane (99/1)	$\Delta T_s \geq 9.5K$	8.415715	4.340422×10^{-5}	$-1.416185 \times 10^{-10}$	$-6.081541 \times 10^{-16}$
	$\Delta T_s \leq 9.5K$	-8.193729	1.975566×10^{-3}	-7.828415×10^{-8}	1.061641×10^{-12}
R123/heptane (99.5/0.5)	$\Delta T_s \geq 10K$	7.642573	1.367339×10^{-4}	-1.968117×10^{-9}	1.071097×10^{-14}
	$\Delta T_s \leq 10.7K$	-4.695406×10^{-1}	8.135101×10^{-4}	-2.198312×10^{-8}	2.182051×10^{-13}
R123/cyclohexane (99.5/0.5)	$\Delta T_s \geq 9K$	5.140536	2.582199×10^{-4}	-4.229872×10^{-9}	2.413322×10^{-14}
	$\Delta T_s \leq 9K$	-3.819449	1.137466×10^{-3}	-2.584559×10^{-8}	2.736247×10^{-15}
R123/cyclohexane (99/1)	$\Delta T_s \geq 0K$	3.727304	3.204812×10^{-4}	-5.075217×10^{-9}	2.809359×10^{-14}
R123	$\Delta T_s \geq 9K$	6.21063	1.71370×10^{-4}	-2.475810×10^{-9}	1.287840×10^{-14}
	$\Delta T_s \leq 9.7K$	-3.71984	1.21909×10^{-3}	-3.952890×10^{-8}	4.497650×10^{-13}

Table 5 Residual standard deviation of q'' data from the mean ΔT_s

Fluid	Low q'' U (K)	High q'' U (K)
R123/isopentane (99.9/0.1)	(<9.5K) 0.18	(>8.5K) 0.13
R123/isopentane (99.5/0.5)	(<9.5K) 0.12	(>8K) 0.10
R123/isopentane (99/1)	(<10K) 0.18	(>0K) 0.12
R123/pentane (99.5/0.5)	(<9.7K) 0.26	(>9.7K) 0.04
R123/pentane (99/1)	(<9K) 0.21	(>9K) 0.08
R123/hexane (99.5/0.5)	(<9K) 0.13	(>9K) 0.11
R123/hexane (99/1)	(<9.5K) 0.15	(>9.5K) 0.06
R123/heptane (99.5/0.5)	(<10.7K) 0.16	(>10K) 0.08
R123/cyclohexane (99.5/0.5)	(<9K) 0.19	(>9K) 0.10
R123/cyclohexane (99/1)	(<0K) 0.14	(>0K) 0.14
R123	(<9.7K) 0.25	(>9K) 0.11

Table 6 Average magnitude of 95% multi-use confidence interval for mean $T_w - T_s$ (K)

Fluid	Low q'' U (K)	High q'' U (K)
R123/isopentane (99.9/0.1)	0.16	0.07
R123/isopentane (99.5/0.5)	0.13	0.06
R123/isopentane (99/1)	0.21	0.10
R123/pentane (99.5/0.5)	0.24	0.04
R123/pentane (99/1)	0.22	0.07
R123/hexane (99.5/0.5)	0.15	0.04
R123/hexane (99/1)	0.13	0.04
R123/heptane (99.5/0.5)	0.15	0.06
R123/cyclohexane (99.5/0.5)	0.26	0.06
R123/cyclohexane (99/1)	0.07	0.07
R123	0.15	0.05

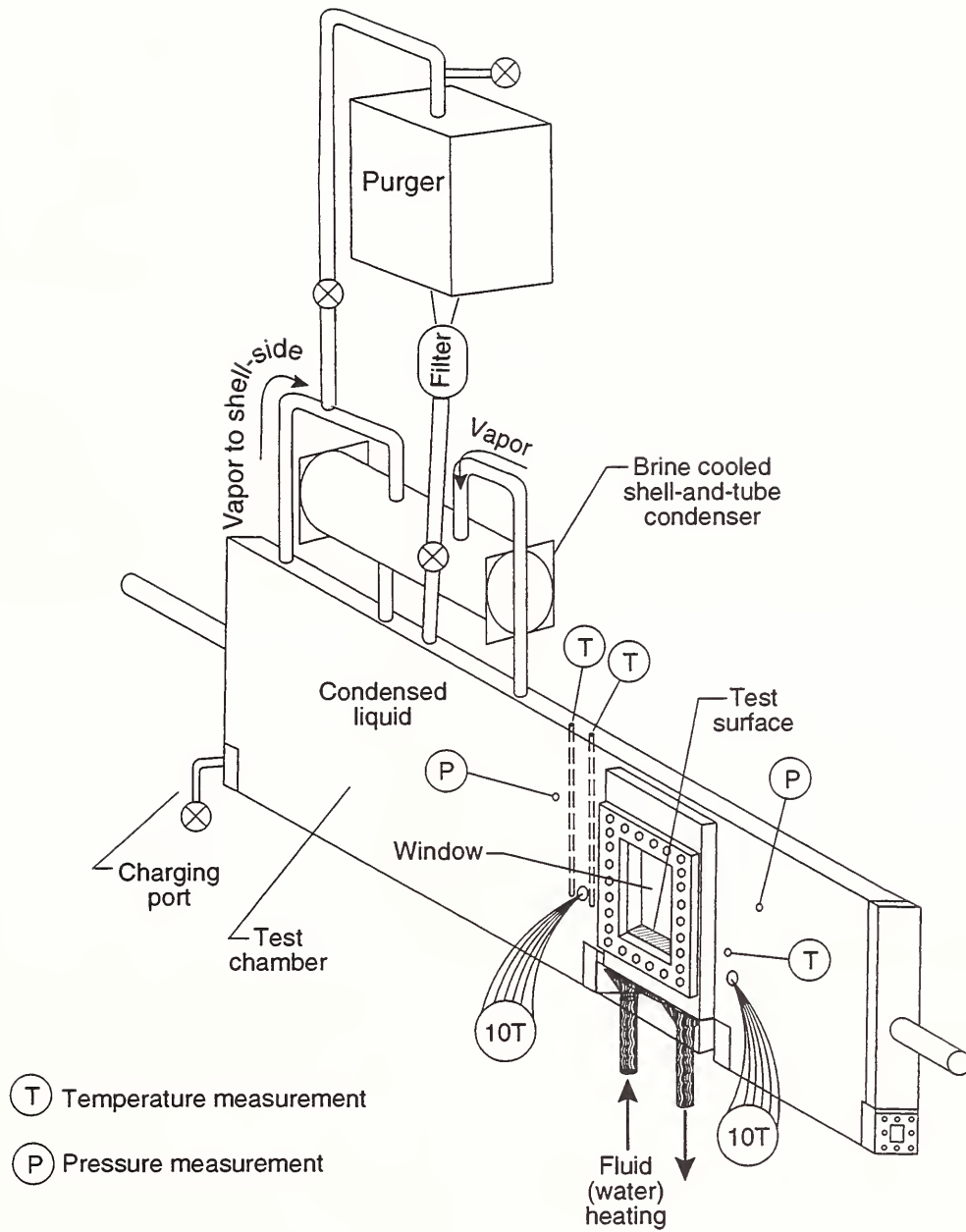


Fig. 1 Schematic of test apparatus

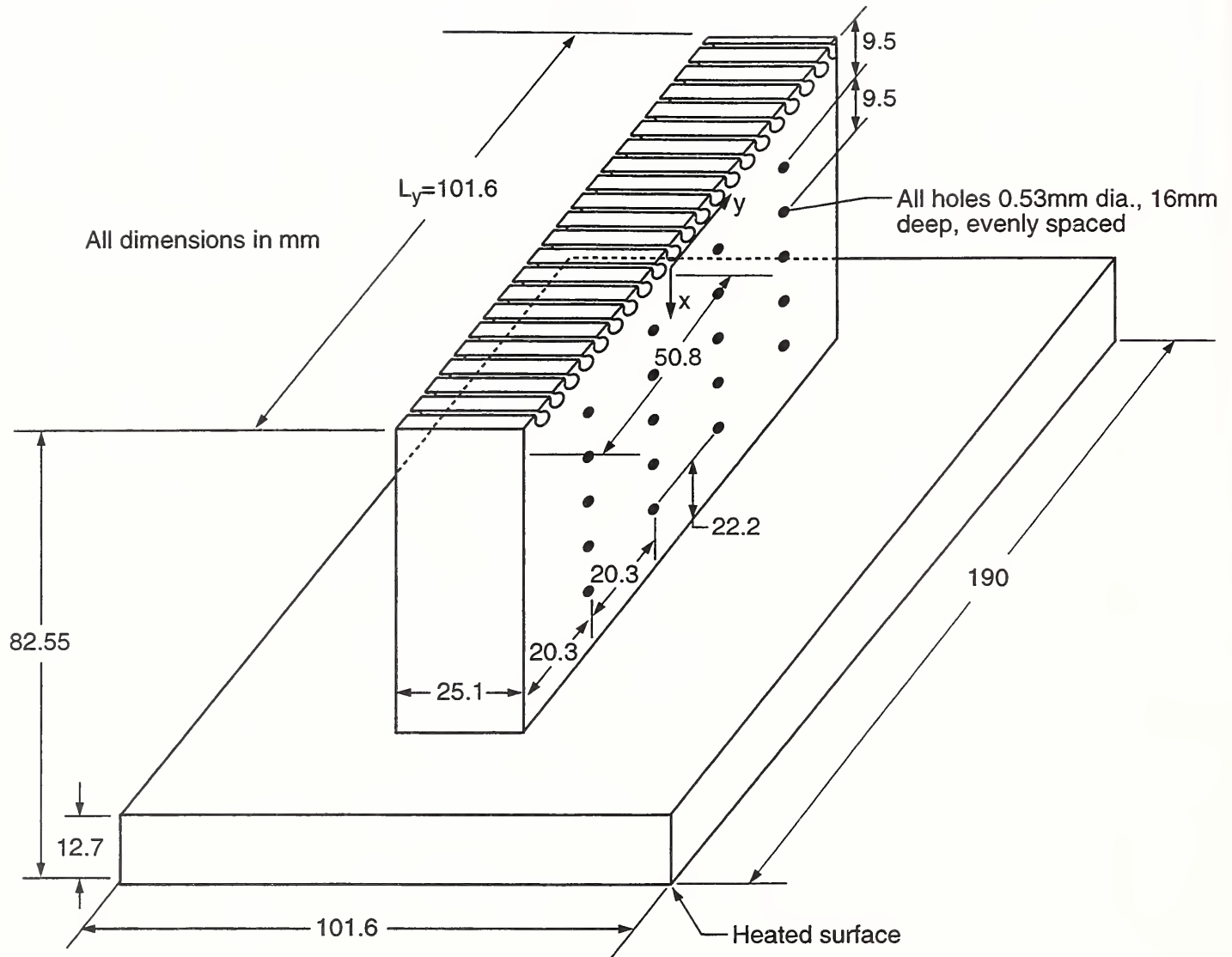
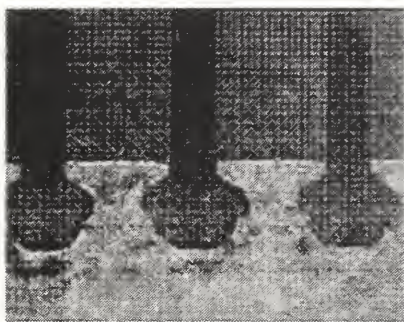
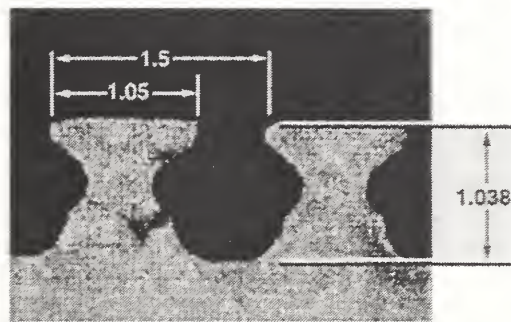


Fig. 2 OFHC copper GEWA-TTM test plate and thermocouple coordinate system



PERSPECTIVE SIDE VIEW



SIDE VIEW

GEWA-T

Fig. 3 Photograph of GEWA-TTM geometry

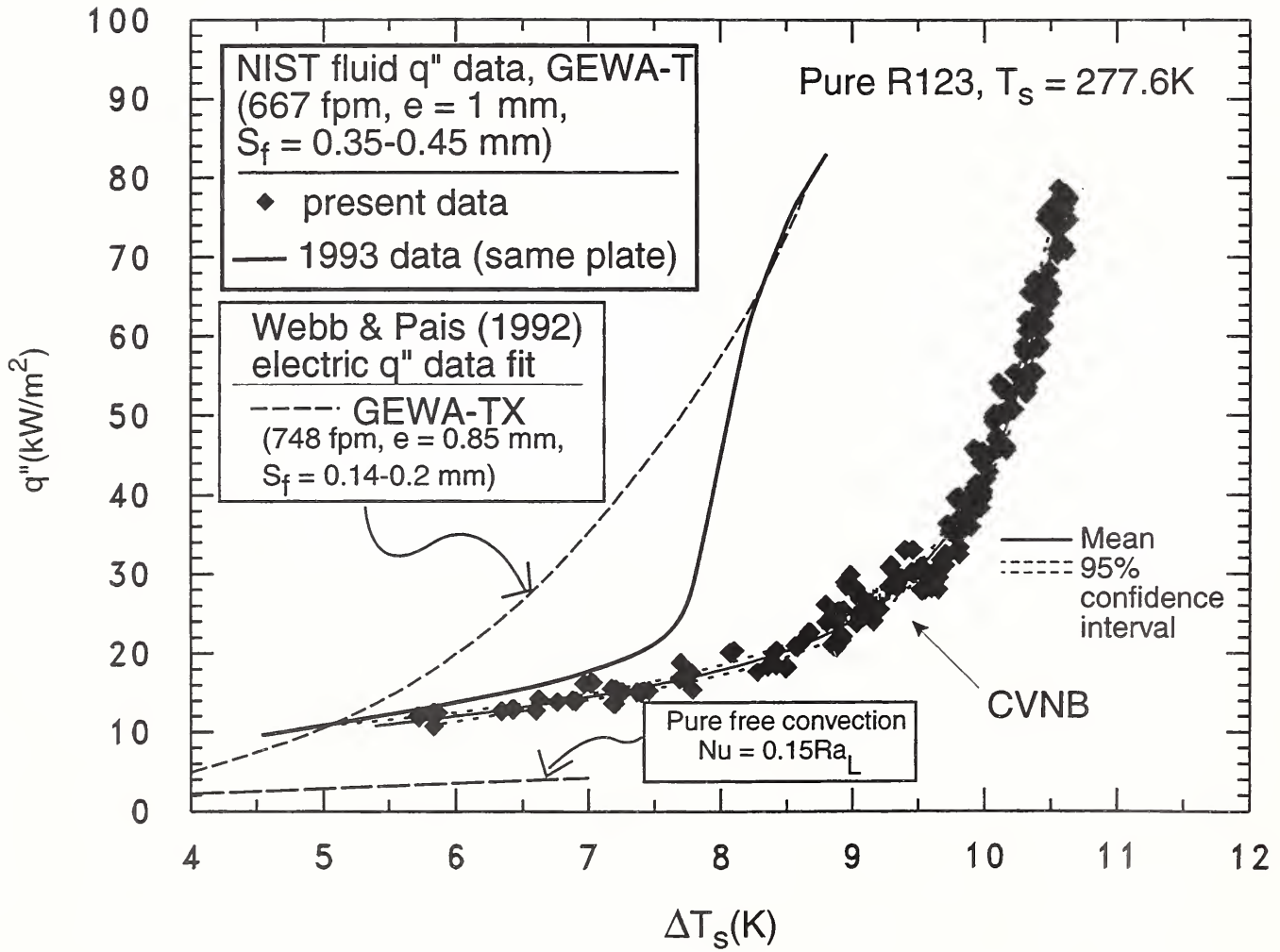


Fig. 4 R123 pool boiling curve for GEWA-T surface at 277.6 K

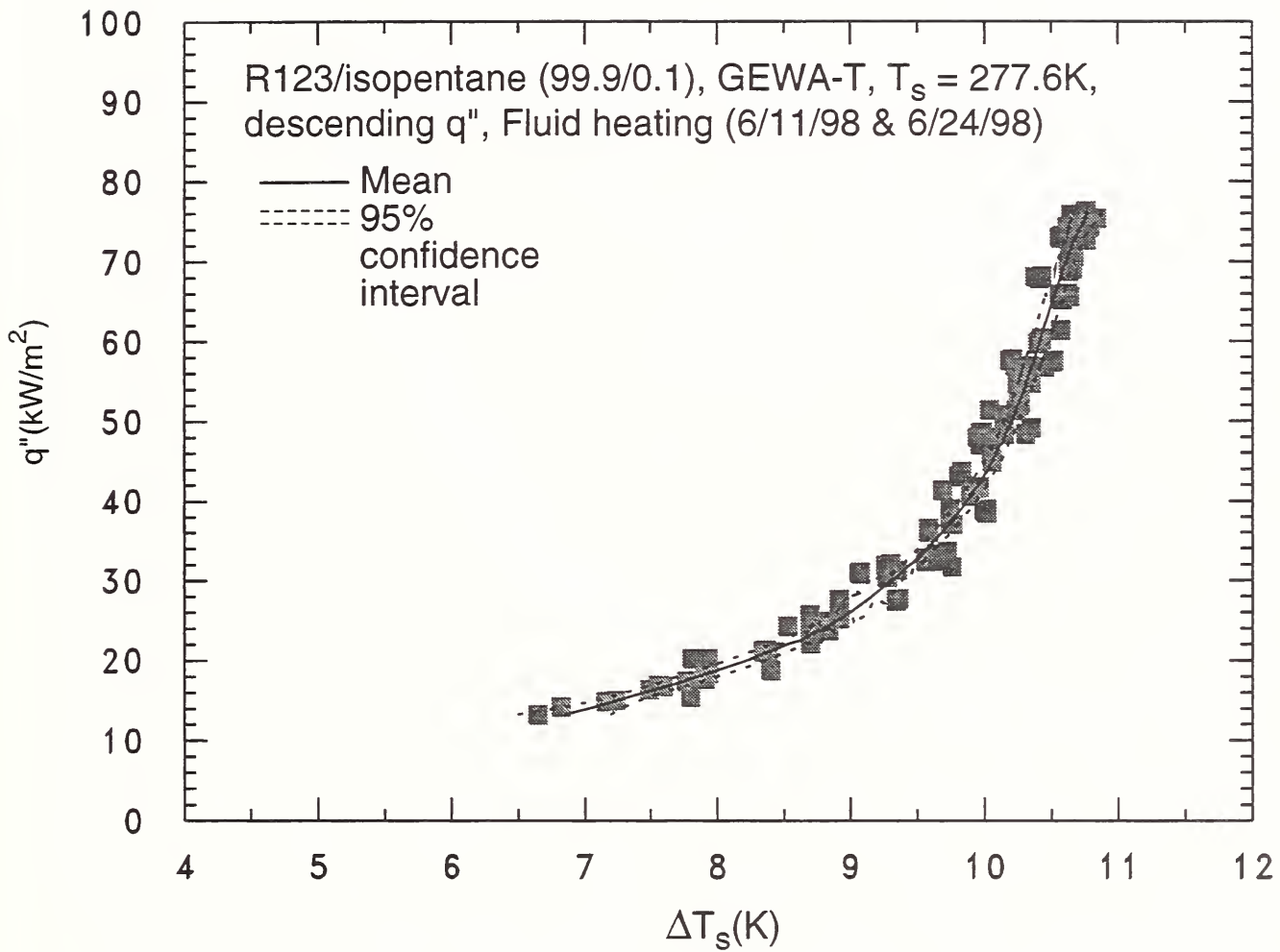


Fig. 5 R123/isopentane (99.9/0.1) pool boiling curve for GEWA-T surface at 277.6 K

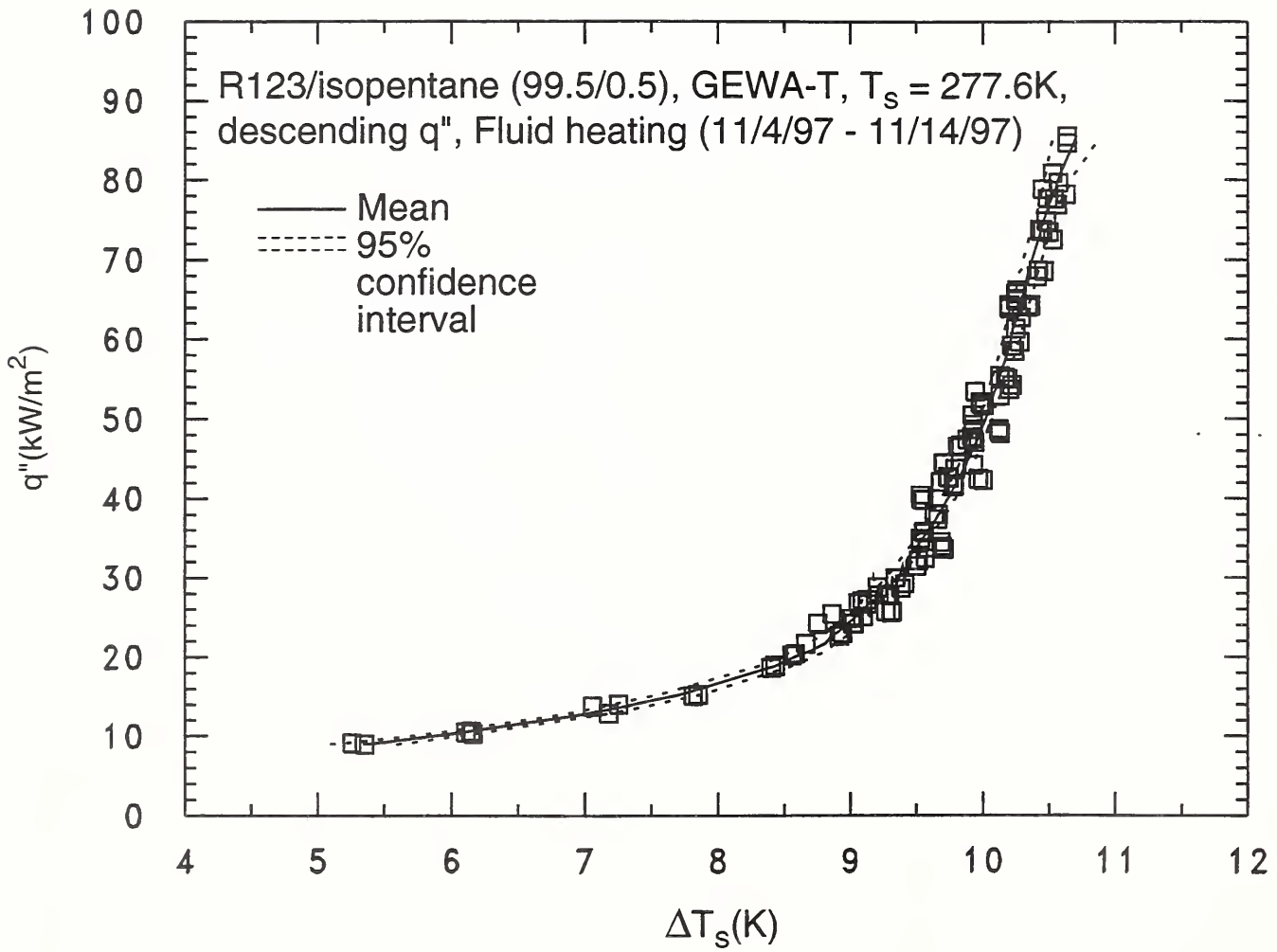


Fig. 6 R123/isopentane (99.5/0.5) pool boiling curve for GEWA-T surface at 277.6 K

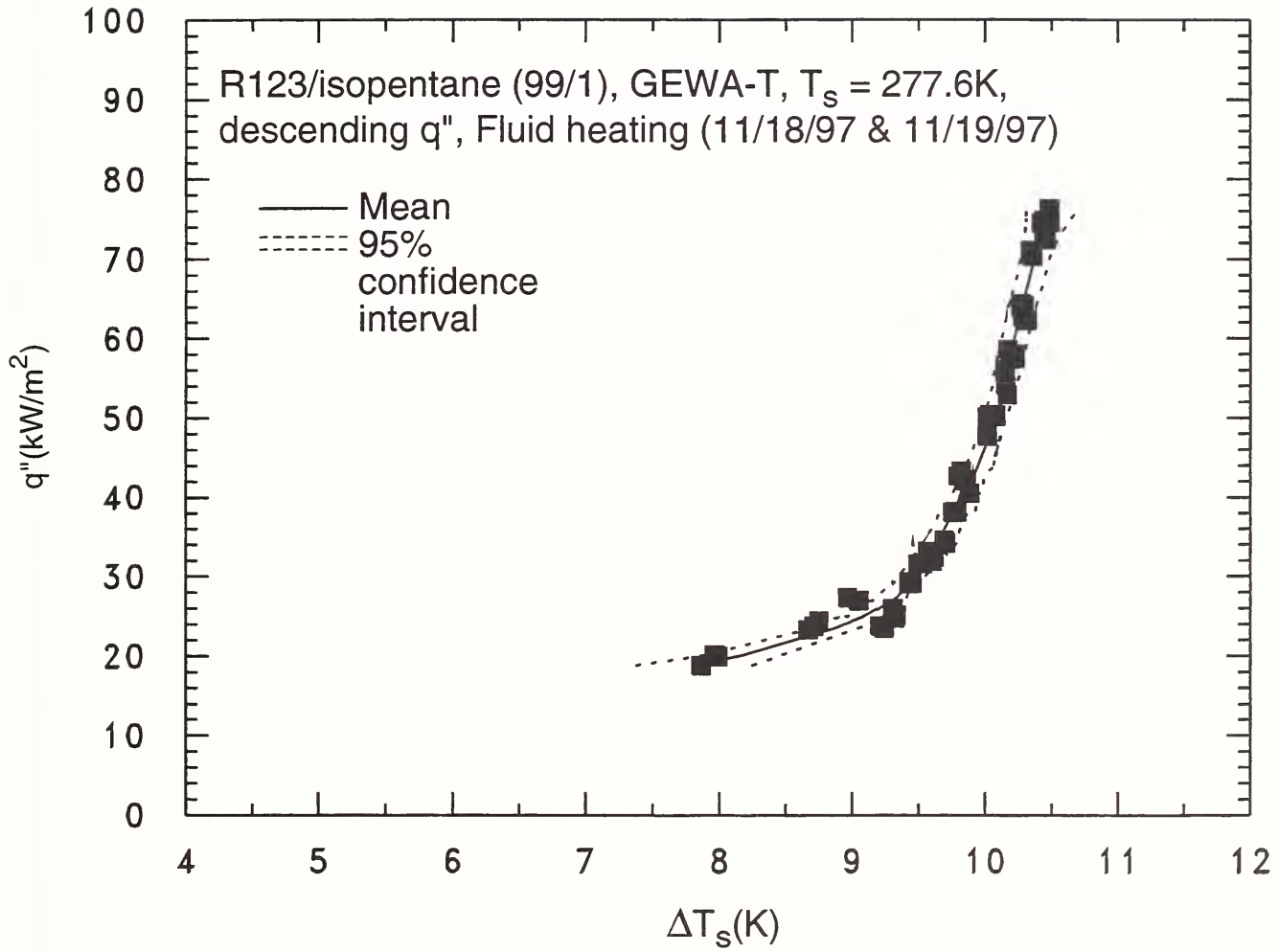


Fig. 7 R123/isopentane (99/1) pool boiling curve for GEWA-T surface at 277.6 K

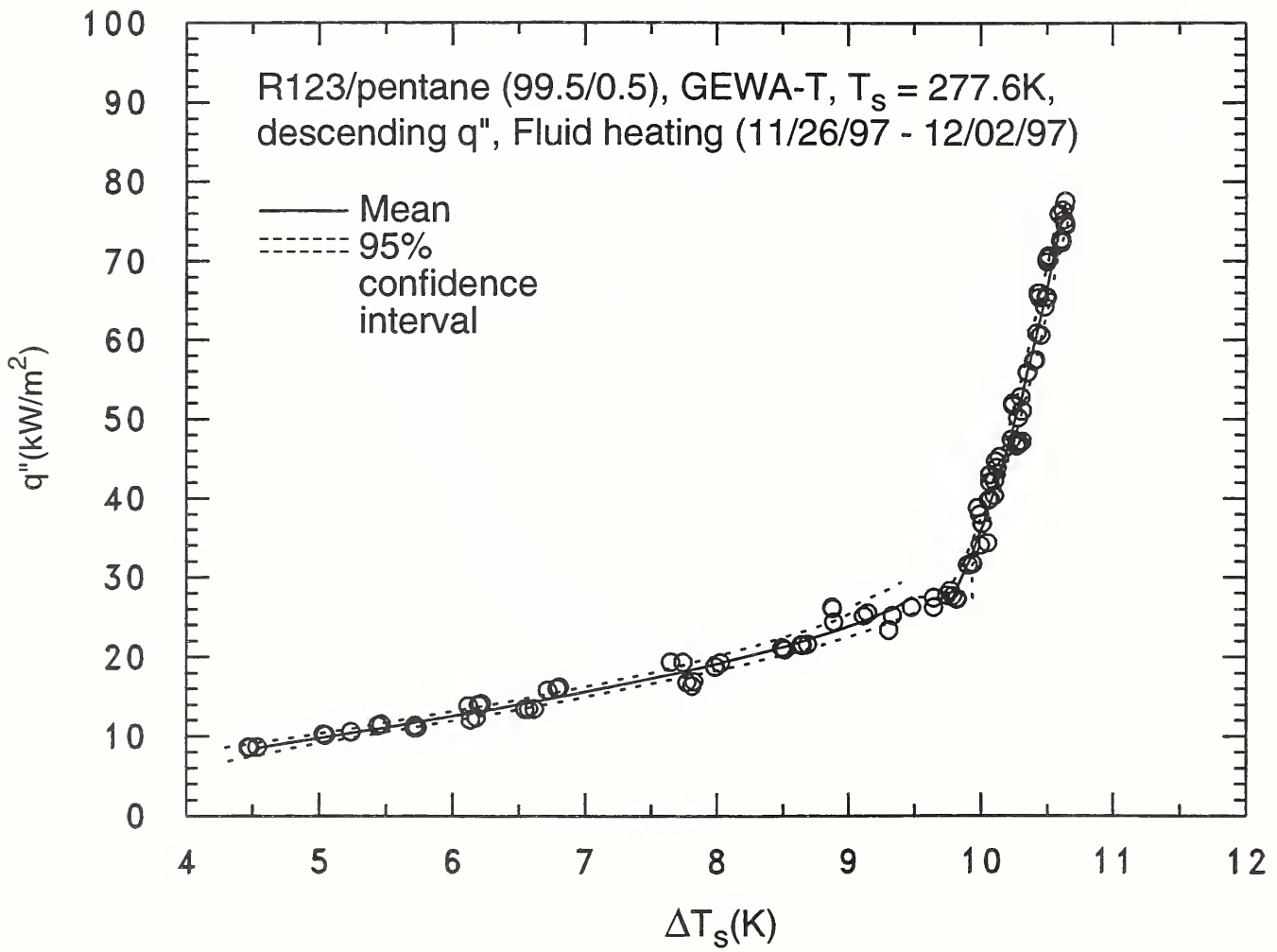


Fig. 8 R123/pentane (99.5/0.5) pool boiling curve for GEWA-T surface at 277.6 K

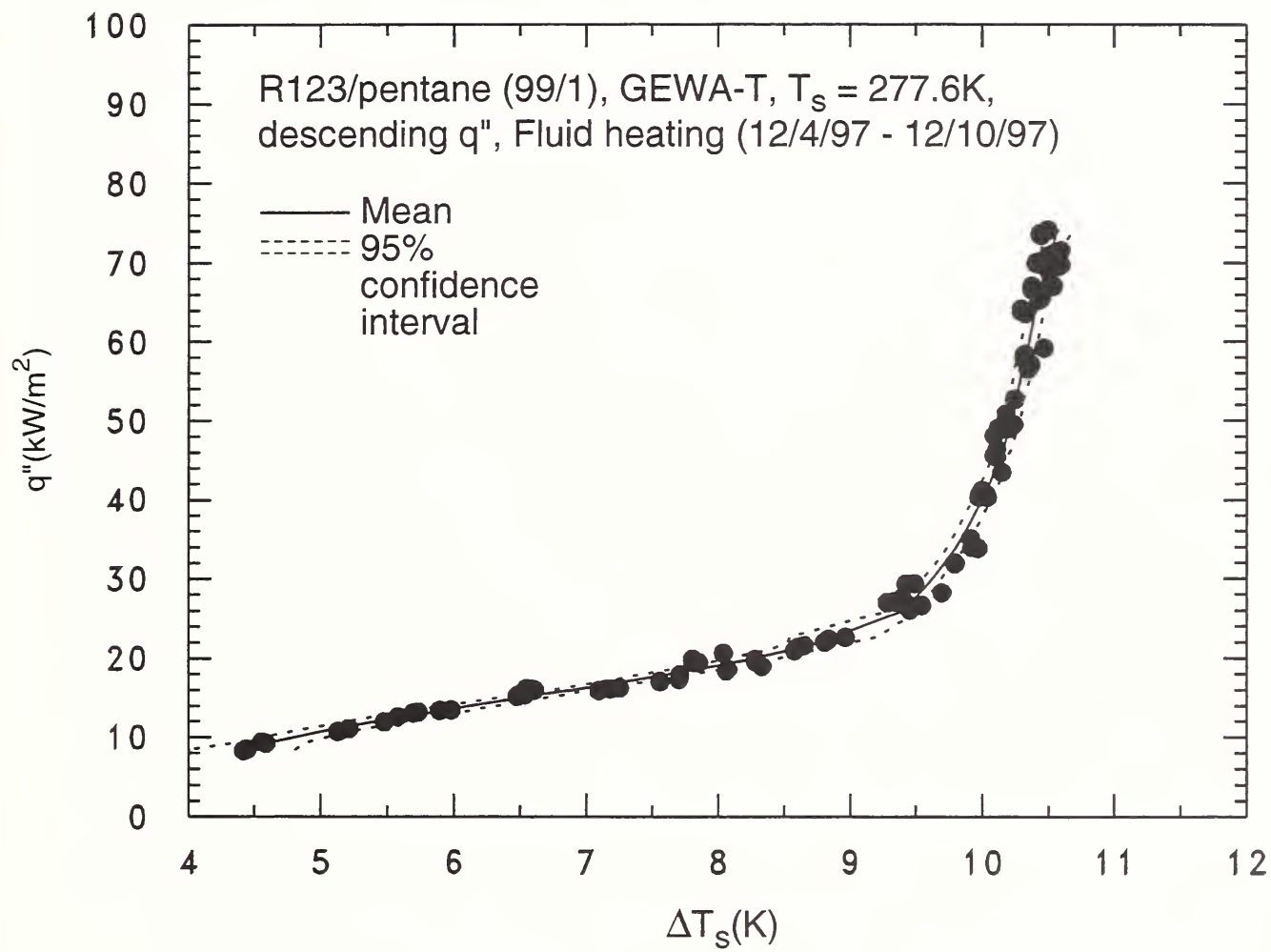


Fig. 9 R123/pentane (99/1) pool boiling curve for GEWA-T surface at 277.6 K

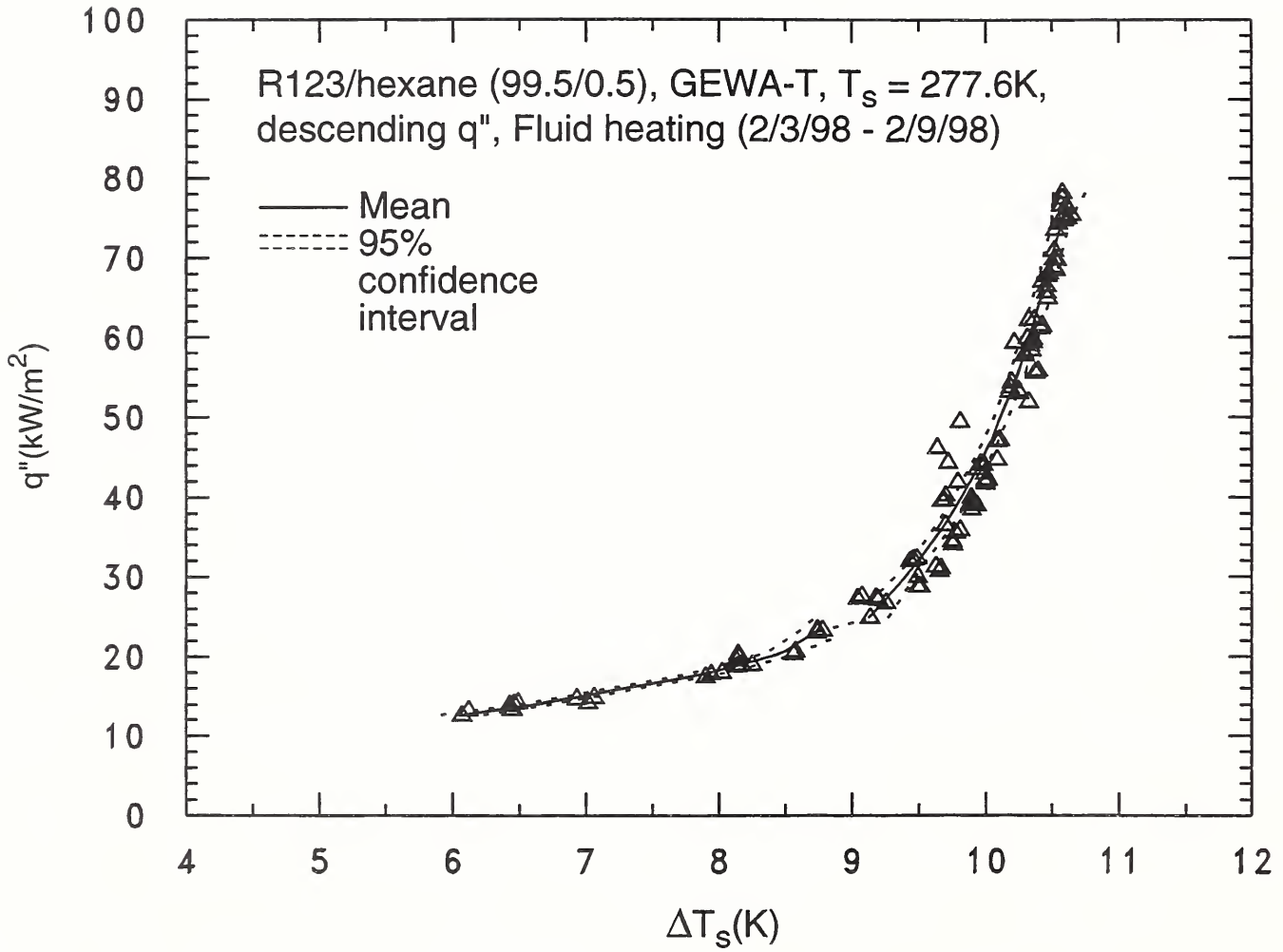


Fig. 10 R123/hexane (99.5/0.5) pool boiling curve for GEWA-T surface at 277.6 K

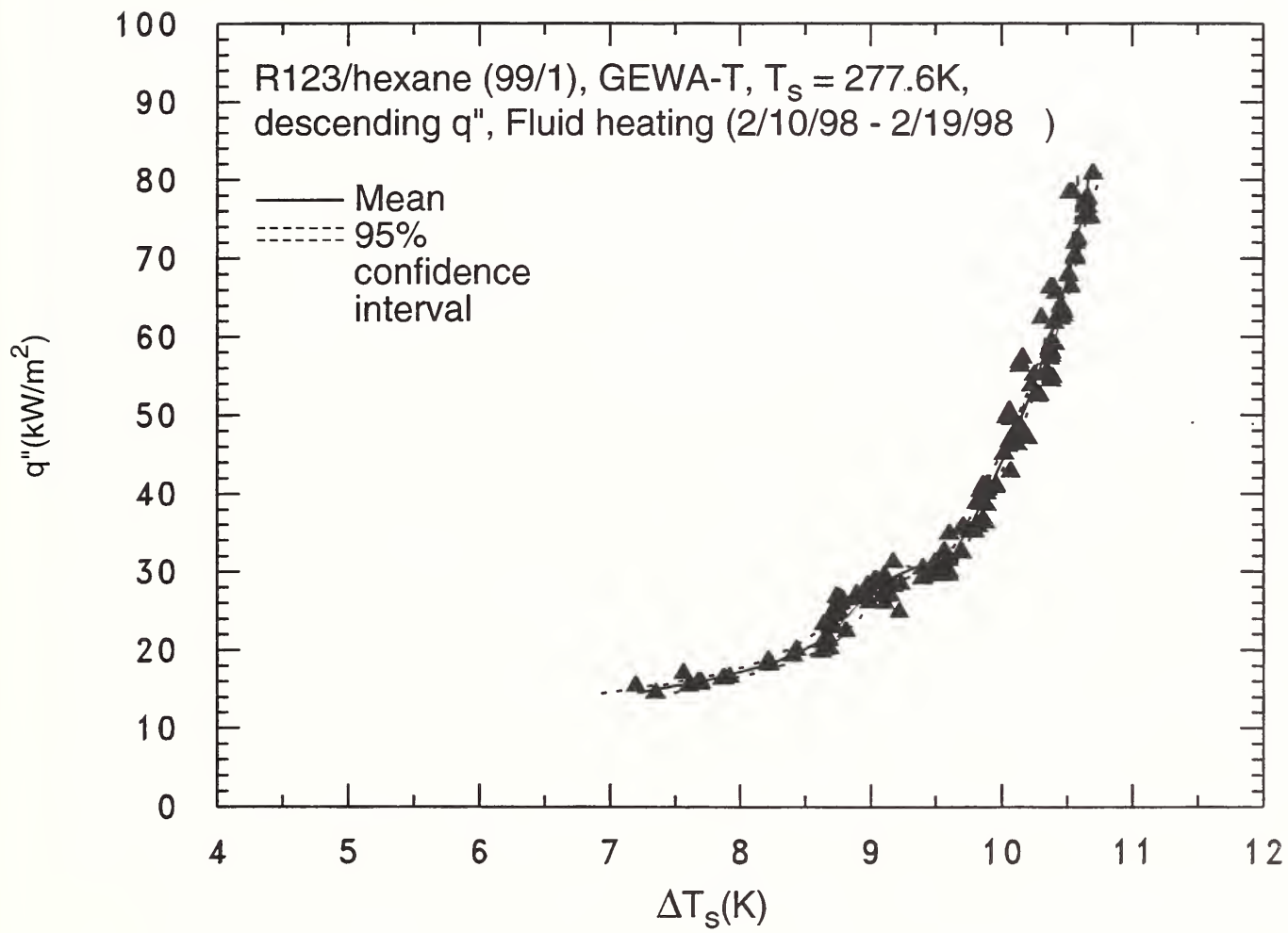


Fig. 11 R123/hexane (99/1) pool boiling curve for GEWA-T surface at 277.6 K

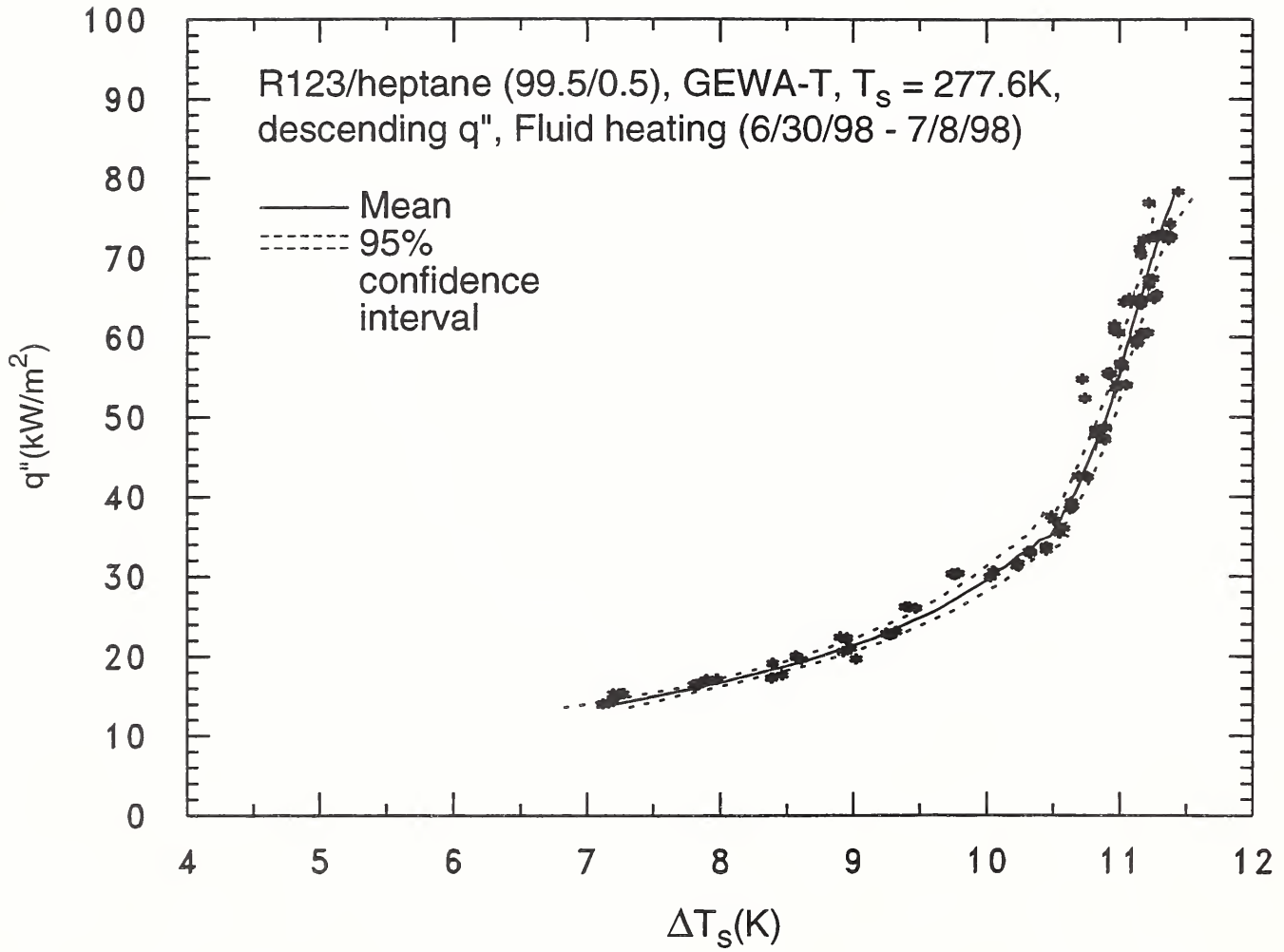


Fig. 12 R123/heptane (99.5/0.5) pool boiling curve for GEWA-T surface at 277.6 K

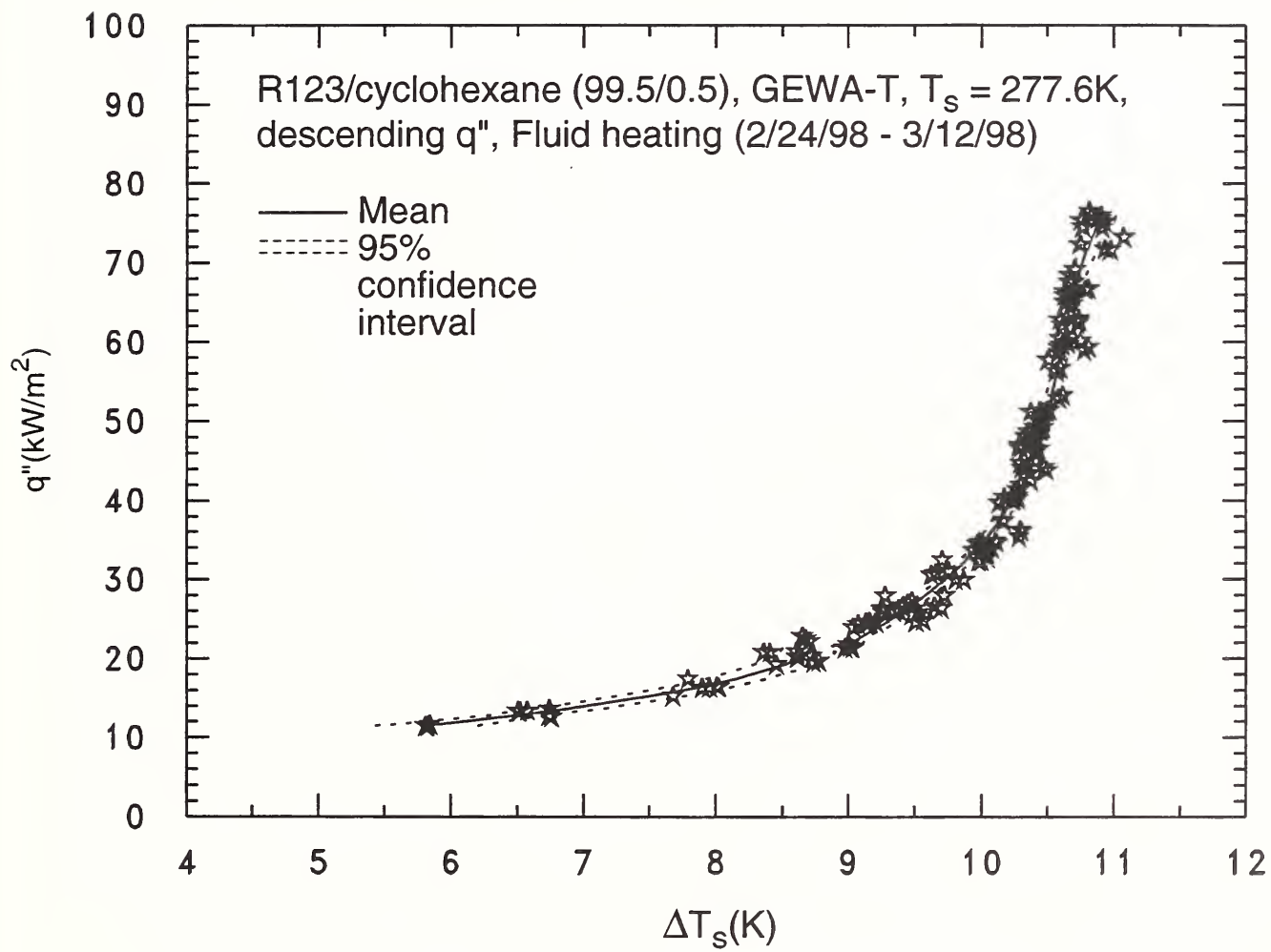


Fig. 13 R123/cyclohexane (99.5/0.5) pool boiling curve for GEWA-T surface at 277.6 K

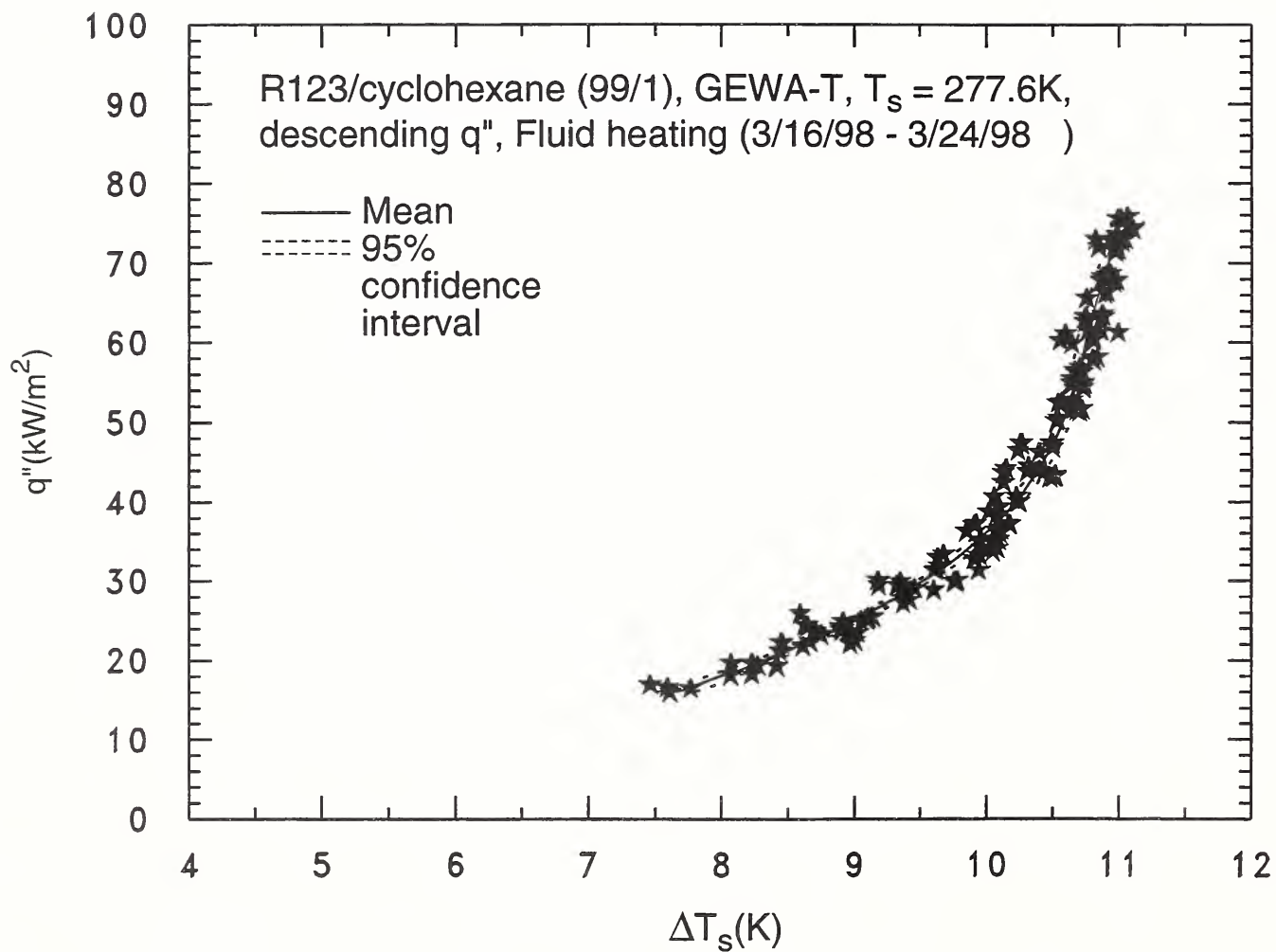


Fig. 14 R123/cyclohexane (99/1) pool boiling curve for GEWA-T surface at 277.6 K

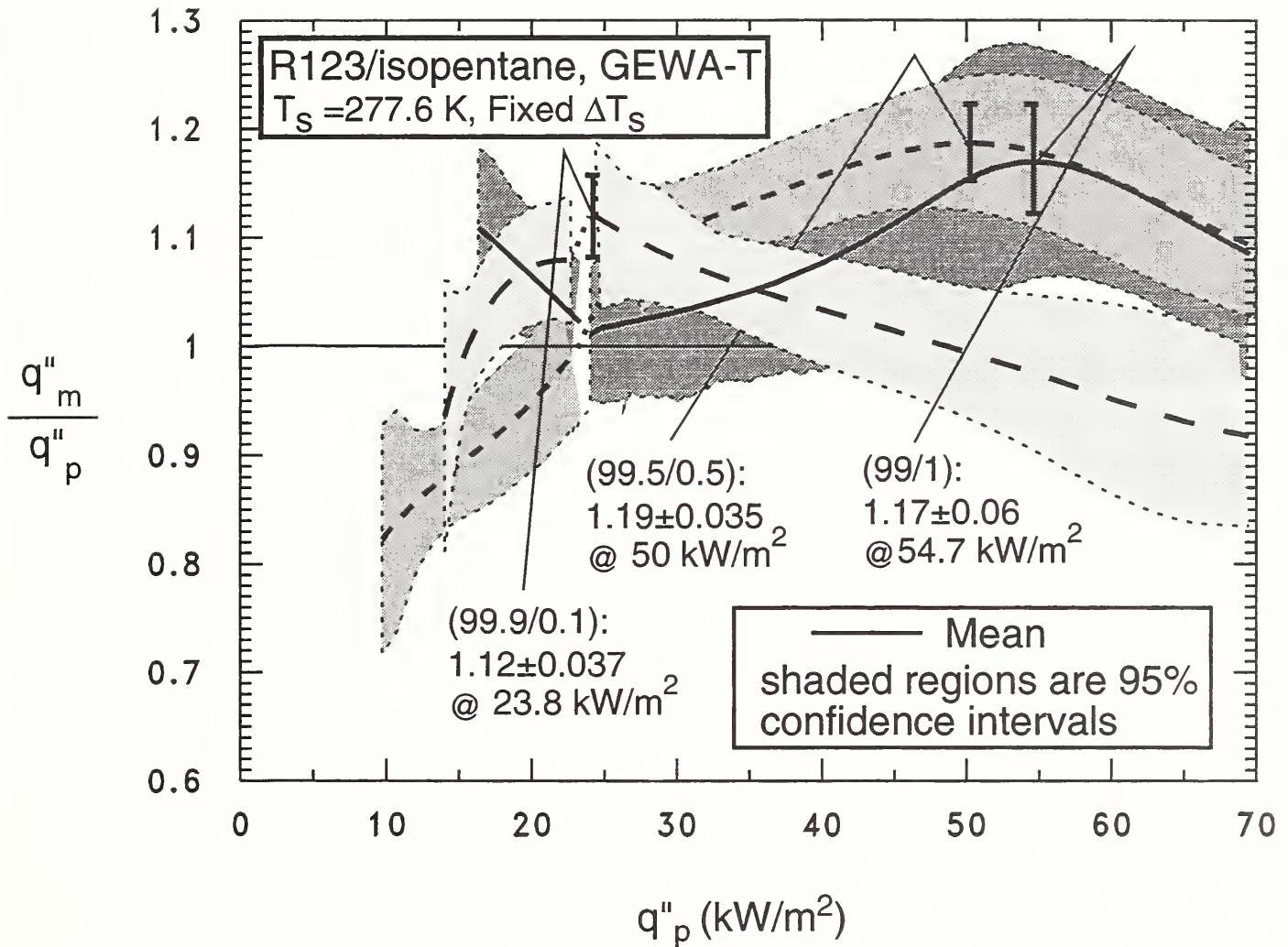


Fig. 15 Enhancement ratio for three dilute R123/isopentane mixtures

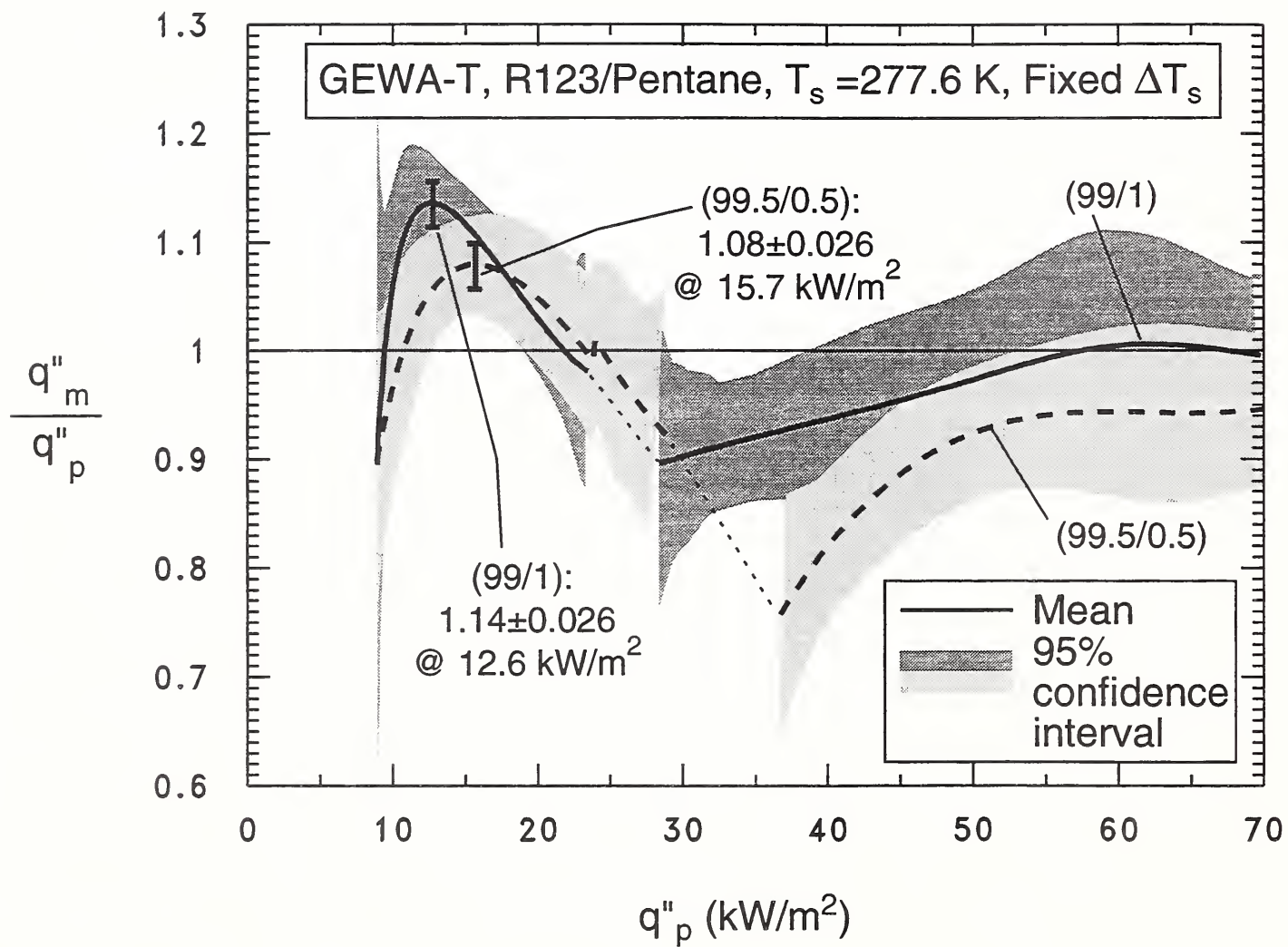


Fig. 16 Enhancement ratio for two dilute R123/pentane mixtures

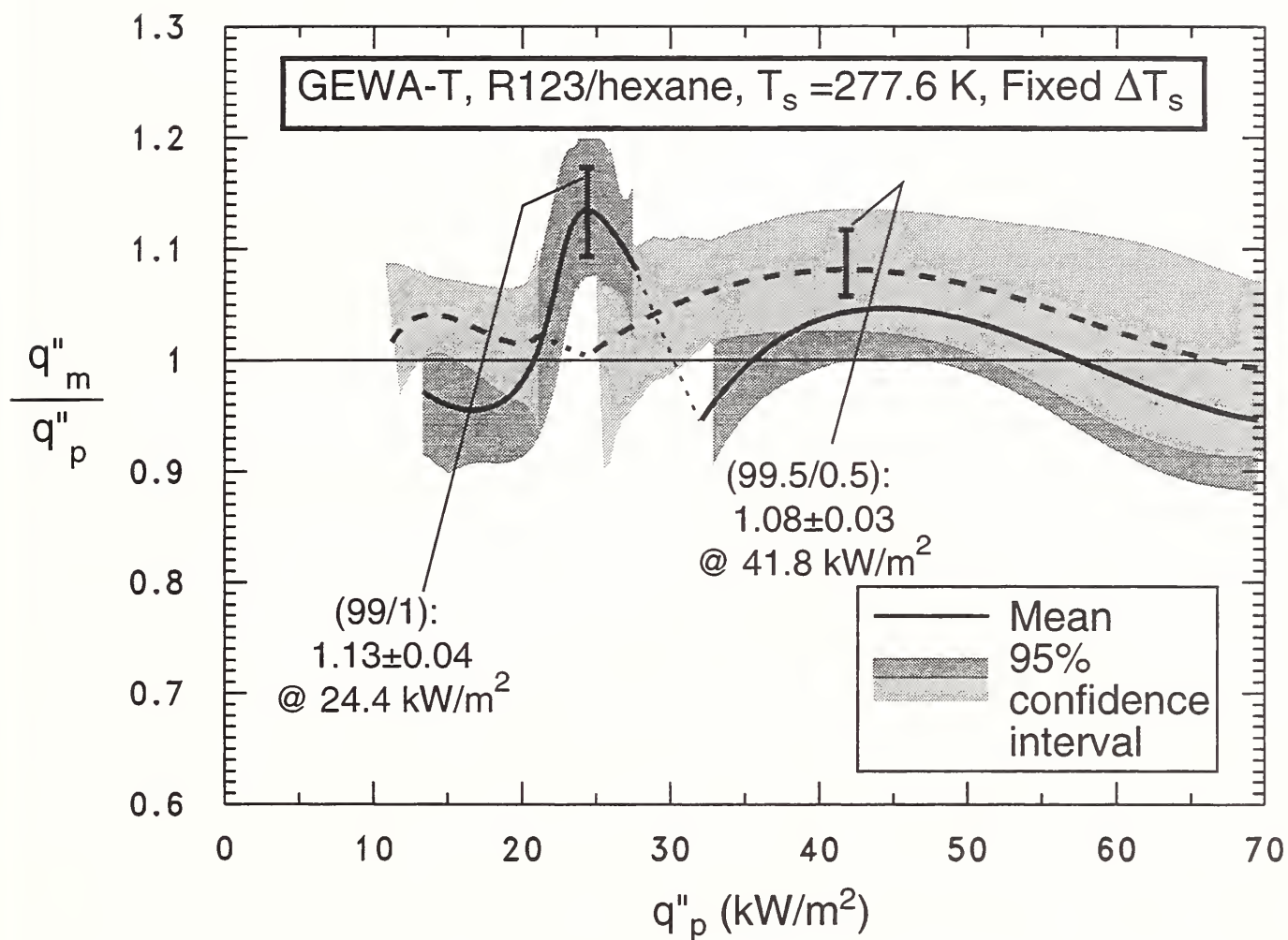


Fig. 17 Enhancement ratio for two dilute R123/hexane mixtures

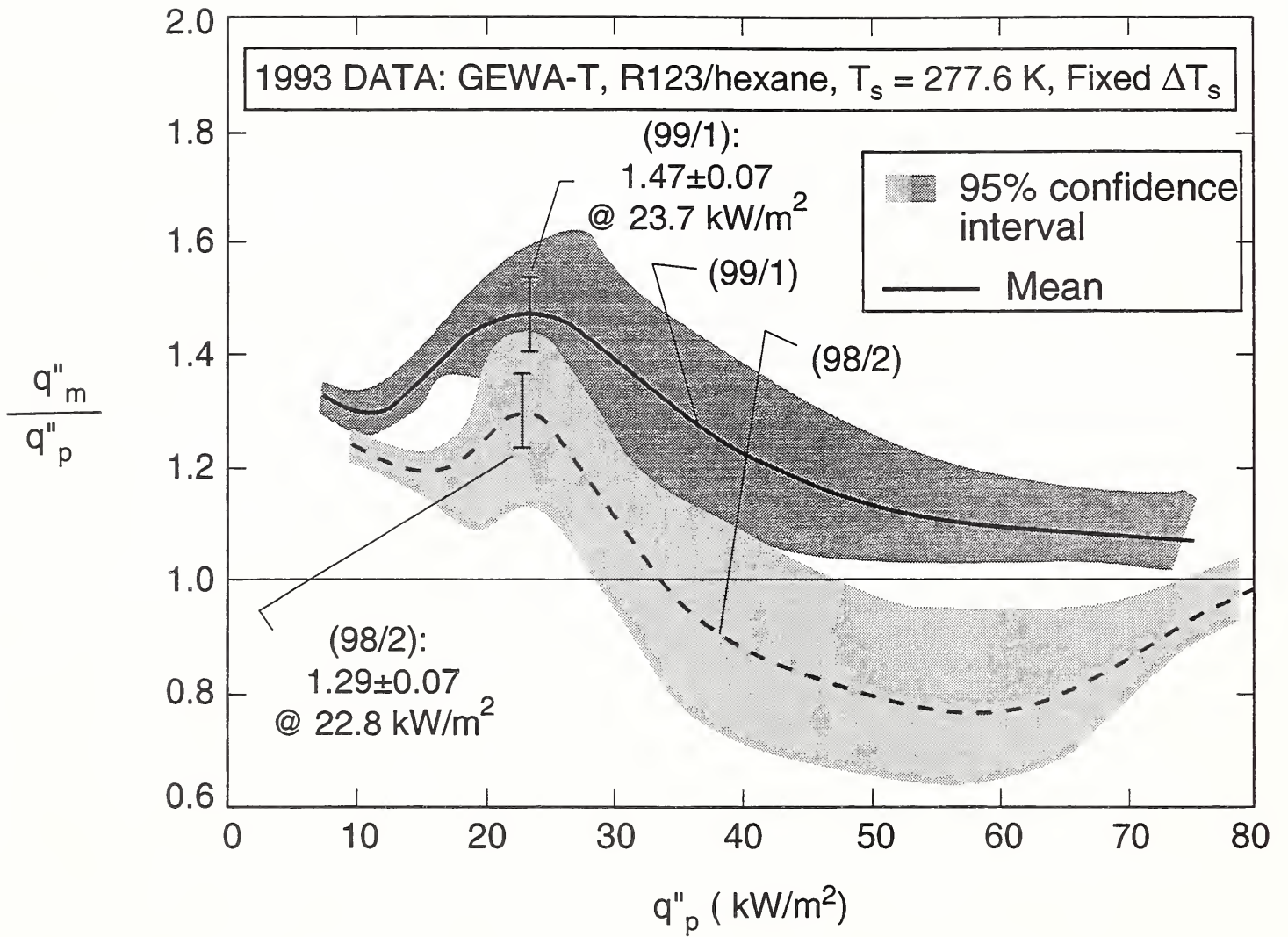


Fig .18 Effect of hexane on R123 pool boiling heat flux as measured in 1993

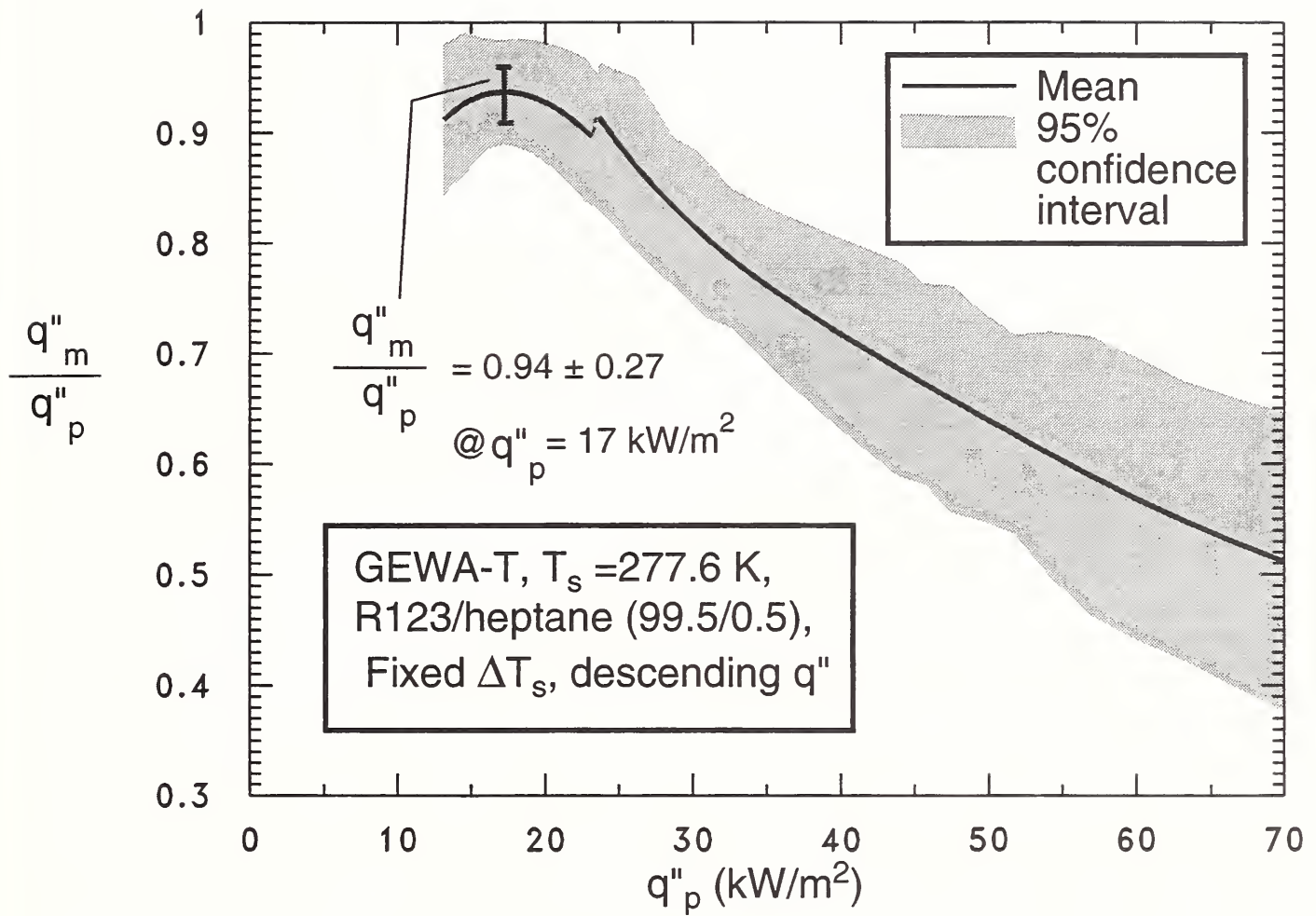


Fig. 19 Enhancement ratio for R123/heptane (99.5/0.5)

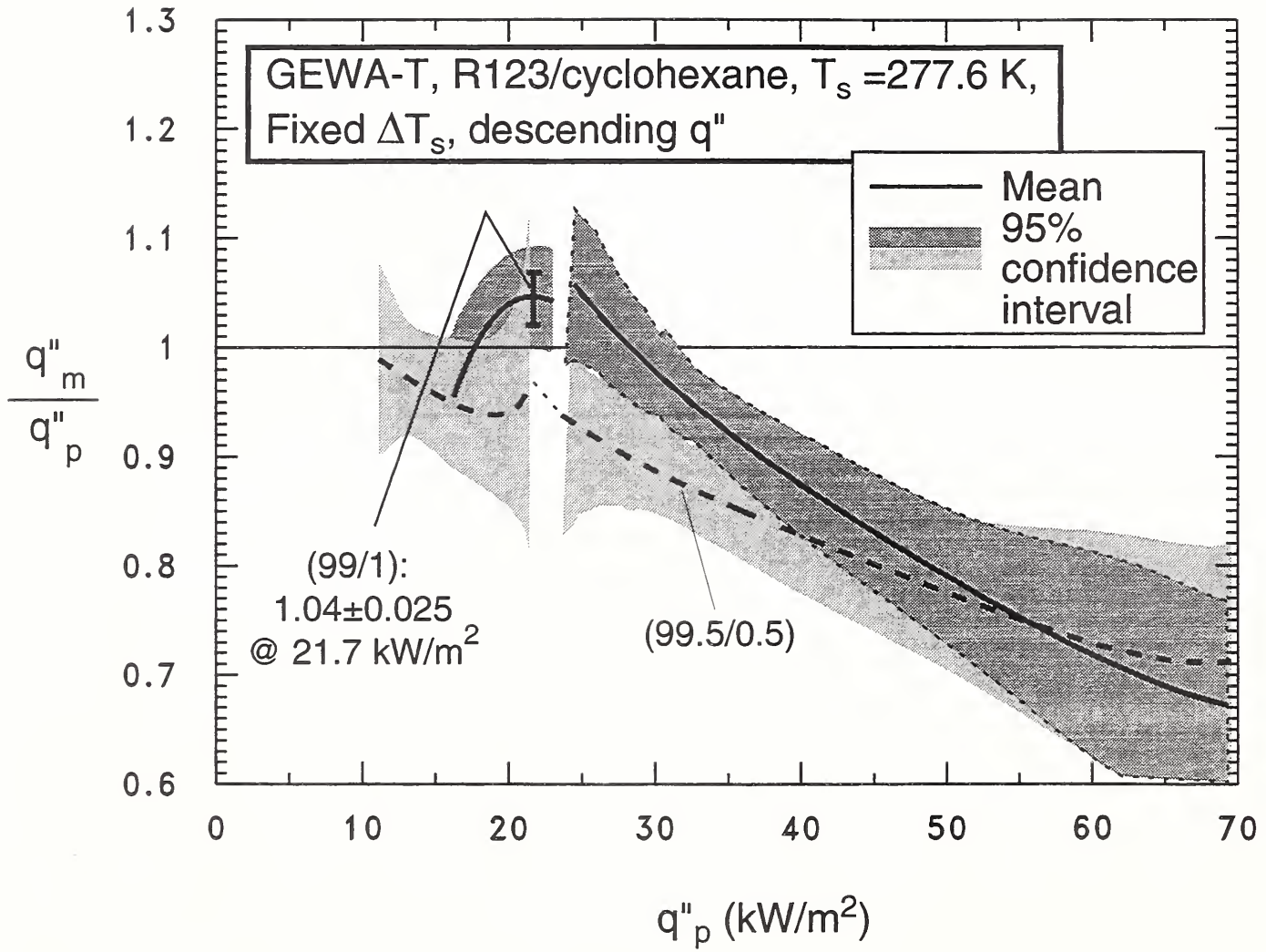


Fig. 20 Enhancement ratio for two dilute R123/cyclohexane mixtures

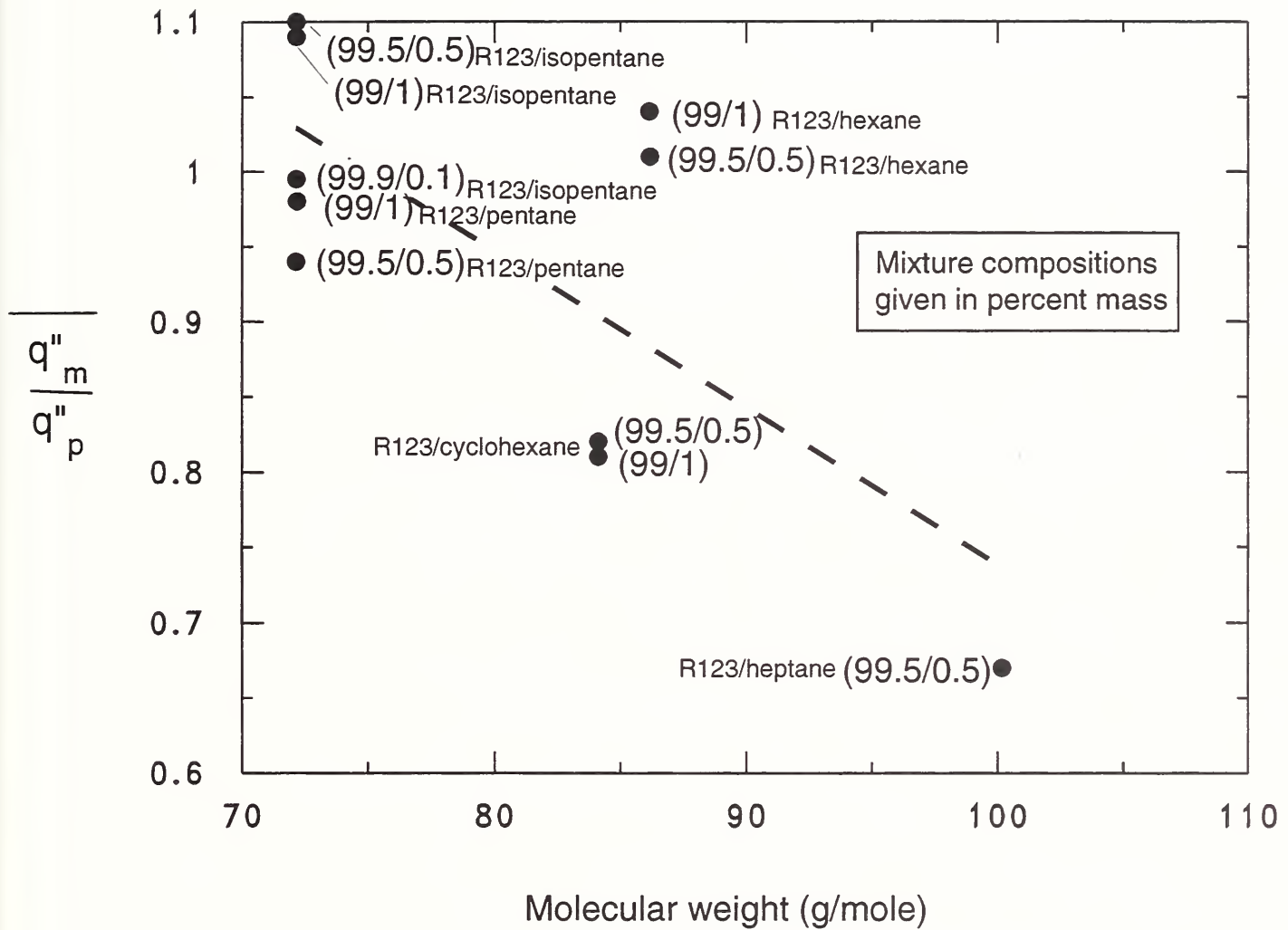


Fig. 21 Influence of molecular weight on the average enhancement ratio for dilute solutions of R123 and hydrocarbons

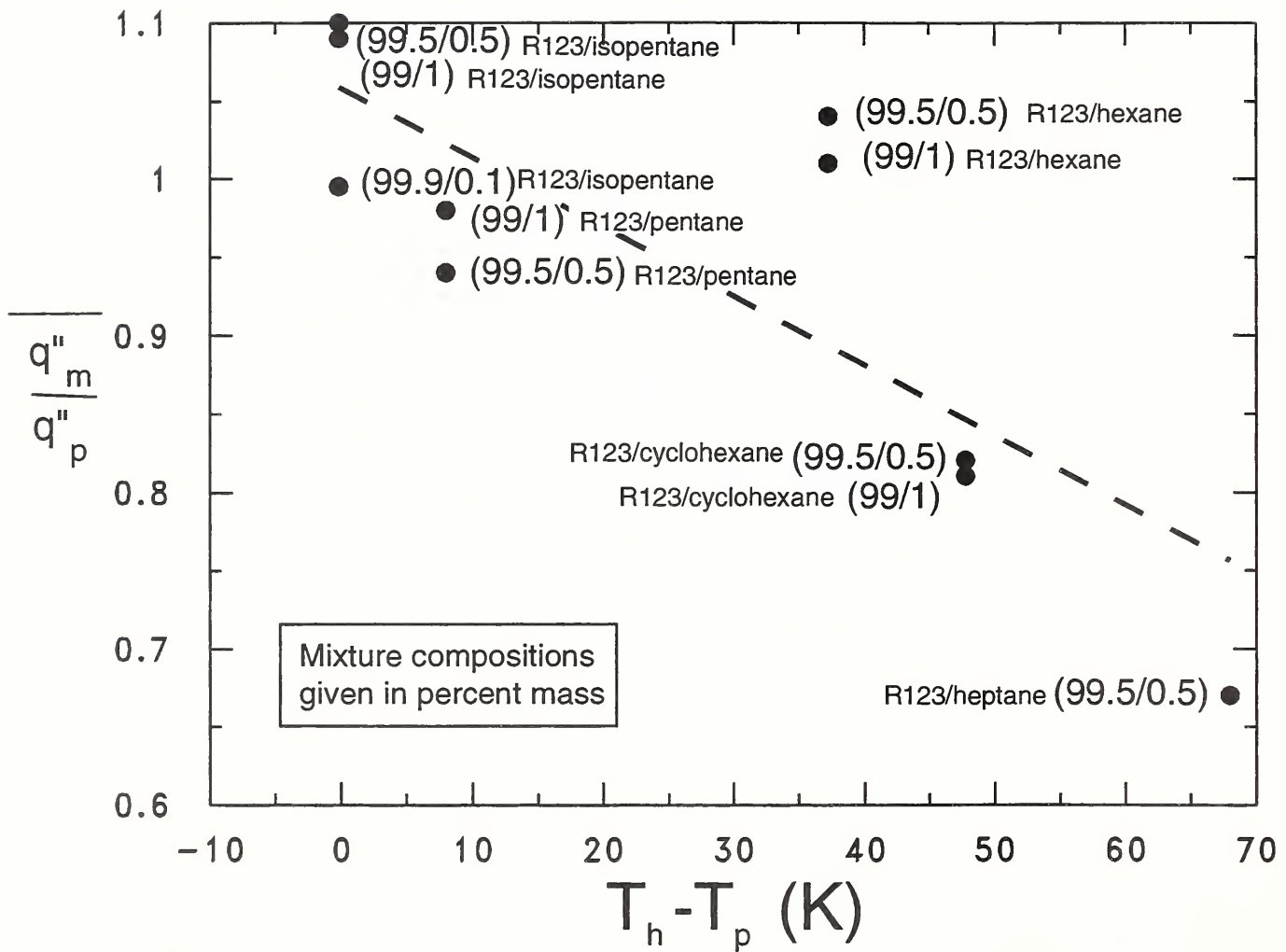


Fig. 22 Influence of boiling range on the average enhancement ratio for dilute solutions of R123 and hydrocarbons

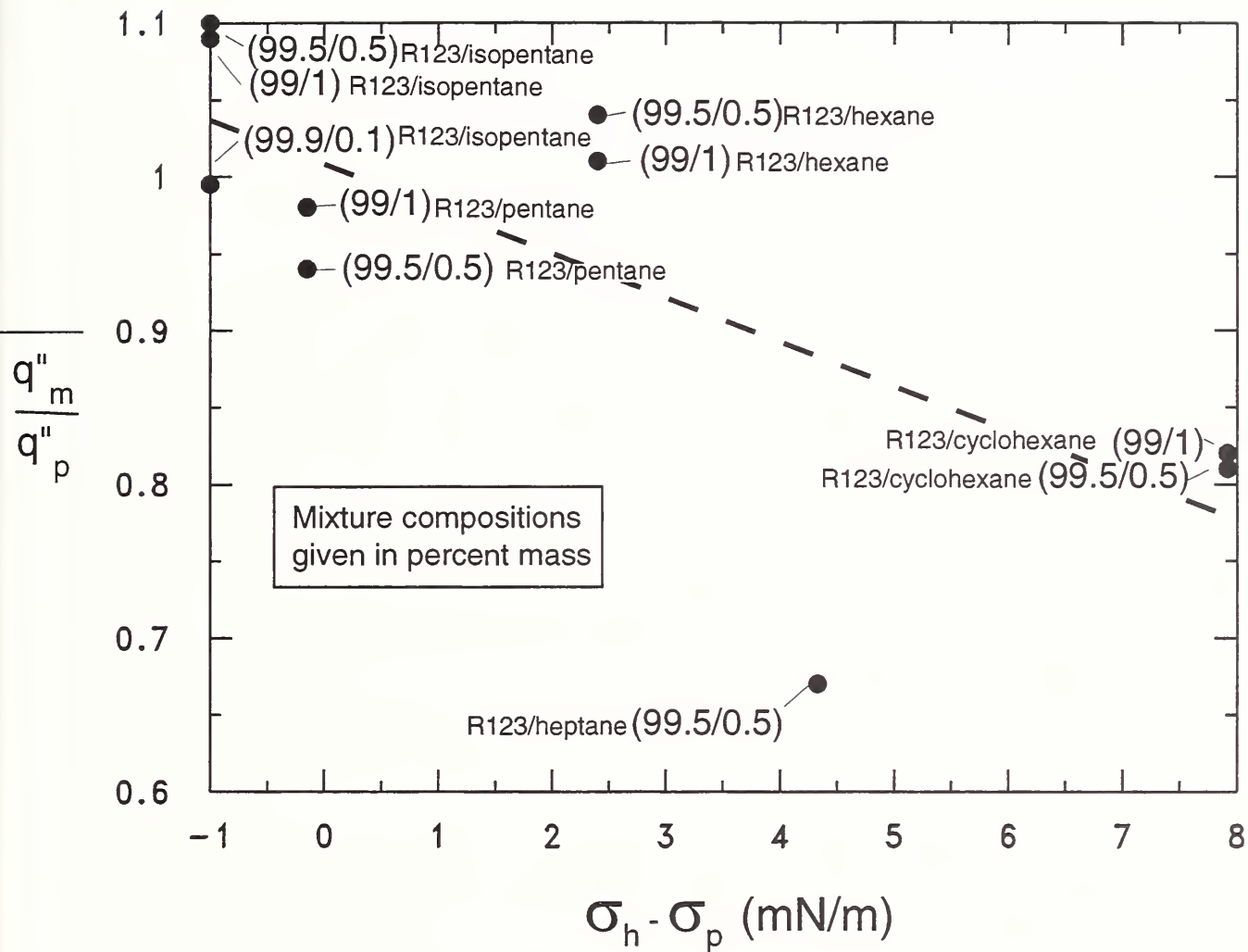


Fig. 23 Influence of surface tension on the average enhancement ratio for dilute solutions of R123 and hydrocarbons

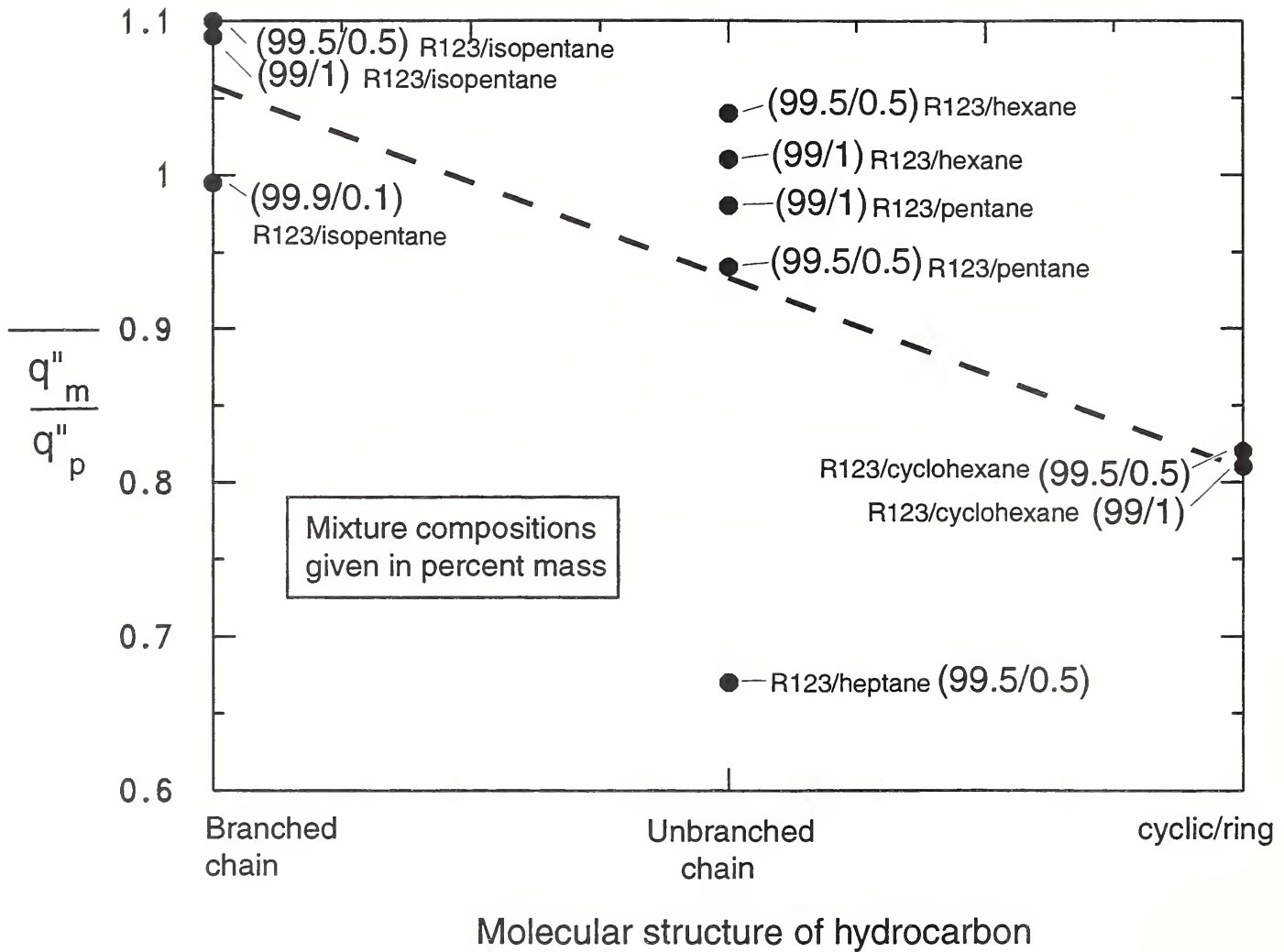


Fig. 24 Influence of molecular structure of hydrocarbon on the average enhancement ratio for dilute solutions of R123 and hydrocarbons

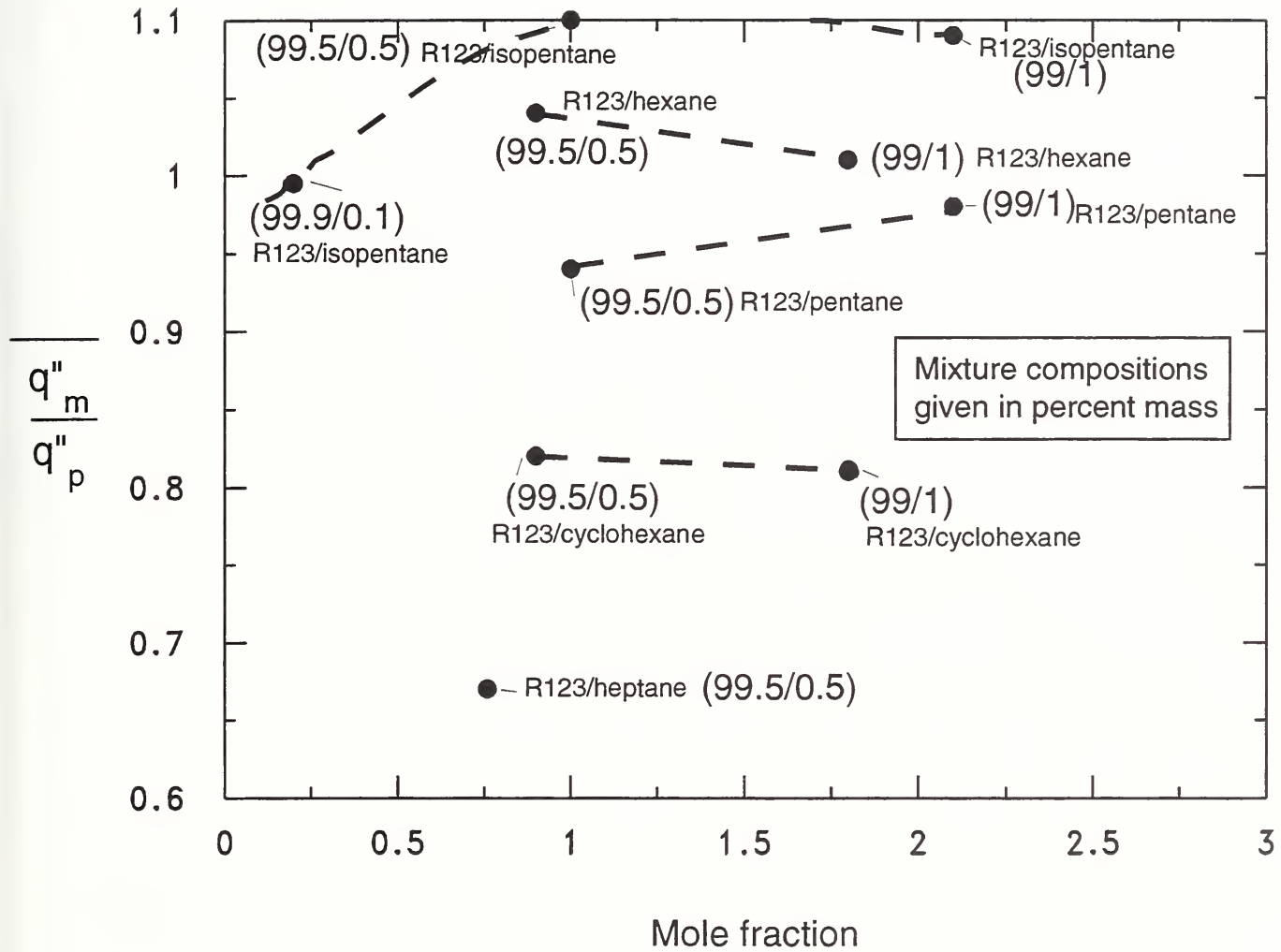


Fig. 25 Influence of mole fraction on the average enhancement ratio for dilute solutions of R123 and hydrocarbons

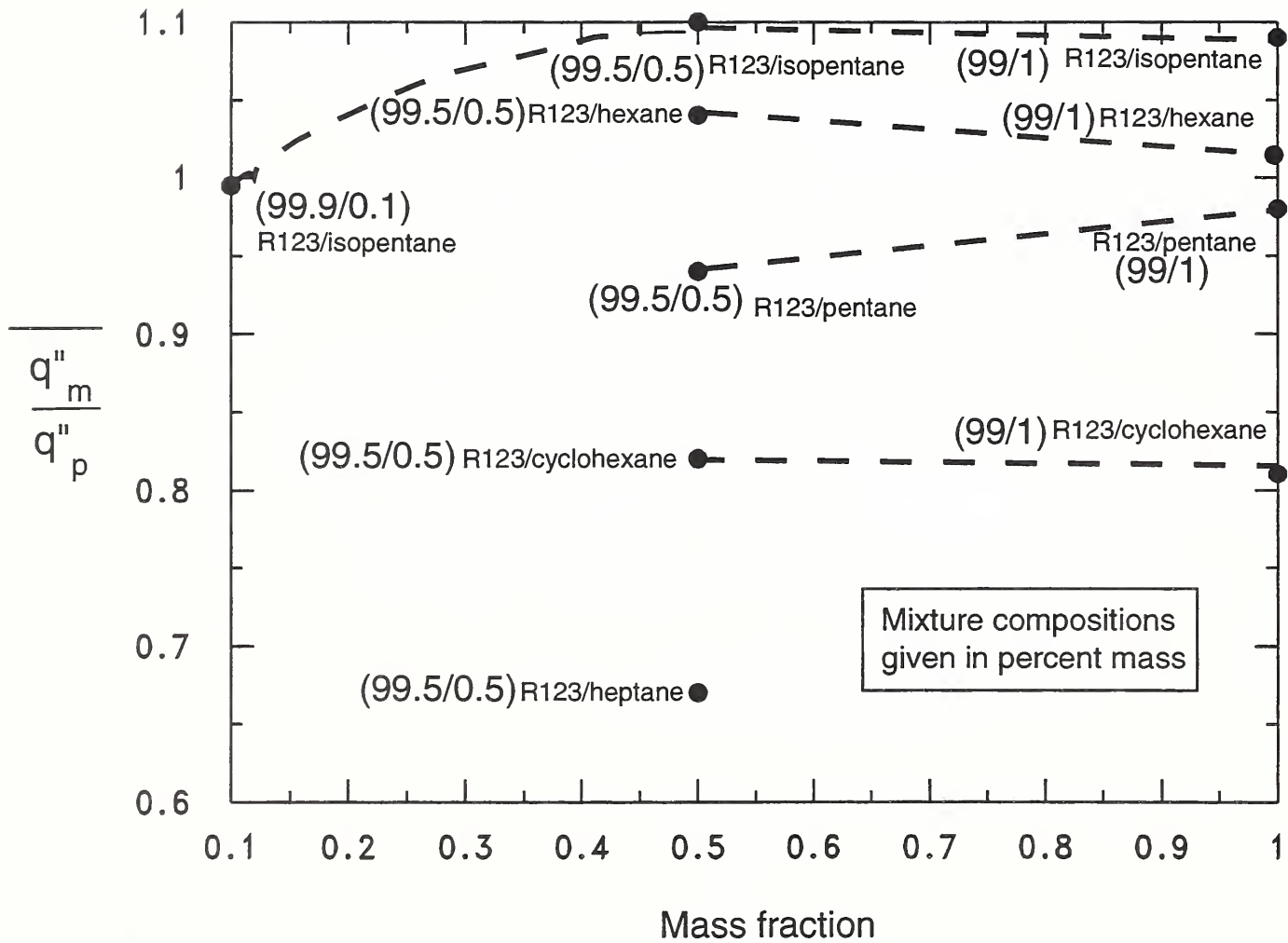


Fig. 26 Influence of mass fraction on the average enhancement ratio for dilute solutions of R123 and hydrocarbons

